Characterizing the Programmatic Response to the Small Molecule Inhibitor, Halofuginol, in a TGFB-Induced Fibroblast

Characterizing the Programmatic Response to the Small Molecule Inhibitor, Halofuginol, in a TGFβ-Induced Fibroblast

Kristen E. Powers

A Thesis in the Field of Biology

for the Degree of Master of Liberal Arts in Extension Studies

Harvard University

May 2019

Abstract

The use of small molecule tRNA-synthetase inhibitors has garnered attention for their ability to act as therapeutics for a variety of diseases. Halofuginone and its less toxic analog, Halofuginol, are tRNA-synthetase inhibitors that are currently being investigated by our lab for their ability to dampen cytokine-driven, pathogenic tissue remodeling programs in diverse tissues. While the molecular target of these molecules has been identified, the mechanism of action remains unclear. It is known that HF can activate the amino acid response (AAR) pathway while hindering cytokine-induced pathogenic tissue remodeling. Our group has found that HF can elicit its therapeutic action, including anti-inflammatory and anti-fibrotic effects, independent of the AAR sensor and effector, general control nonderepressible 2 (GCN2).

The work in this thesis characterized the role of HFol in the pulmonary lung fibroblastic cell line, LL29. In this work Halofuginol was shown to activate the canonical AAR in the pulmonary lung fibroblastic cell line, LL29, by inducing the phosphorylation of GCN2 and eIF2α. Specifically, this project used global transcriptomic and proteomic profiling to characterize the programmatic response to HFol in LL29 cells stimulated with the profibrotic cytokine, TGFβ. We found that HFol can suppress many of the profibrotic transcriptional and translational effects in this system. We also found that in the LL29 cells HFol does not disrupt the TGFβ-induced phosphorylation of Smad proteins. Additionally, we began to characterize the transcriptional effects of HFol that are independent of GCN2 kinase activity. Together, this thesis deepens our current

understanding of how HFol functions to modulate the profibrotic program in a fibroblastic cell line.

Acknowledgments

I would like to, first and foremost, thank my advisor and mentor to this thesis, Dr. Malcolm Whitman. Dr. Whitman allowed me the opportunity to continue my Master's program at Harvard Extension while working full-time in his laboratory as a Research Assistant. His guidance and support over the past four years has been invaluable. I would like to thank Tracy Keller and Jim Morris for their continued support and assistance with the writing of this thesis. I would like to extend my gratitude to the members of the Whitman lab who helped me over the years. Leila, Maja, Minjin, YeonJin, Changqian, Miao, Brendan, Mattia and Chang: our conversations over countless cups of coffee and lab lunches have helped me understand that being a scientist is not a solo endeavor. It takes a team, hard work and determination to see a story come together, and this thesis is no exception. I would like to thank Dr. Kami Ahmad and Dr. Welcome Bender for first accepting me into a laboratory at Harvard Medical School and for providing me with my initial exposure to the many tools and techniques I would use throughout the duration of my program.

I would like to thank my mother for always being there for me. Your love, support and encouragement through this whole process never went unnoticed. It's what drove me to the finish line. To my friends for supporting me along the way and encouraging me at every step. Finally, I would like to thank my boyfriend, Nicholas, for your love and unwavering support through this endeavor. You always know how to make me smile and you constantly remind why I wanted to be a scientist.

Table of Contents

List of Tables

List of Figures

Chapter I.

Introduction

The therapeutic effects of the small molecule inhibitor, Halofuginone.

The purpose of this thesis was to characterize the transcriptional and translational effects of the small molecule inhibitor Halofuginol (HFol), on transforming growth factor-beta (TGFβ)-induced-profibrotic fibroblasts. HFol is the less toxic analog of Halofuginone (HF), a racemic halogenated derivative of *febrifugine*, the active ingredient of the traditional Chinese medicine, Chang Shan (Ryley and Betts 1973). HF was originally synthesized as a less toxic, yet comparably potent, alternative of its precursor (Ryley and Betts 1973). In 2012 our group established that Halofuginone competitively and specifically inhibits proline from binding to the prolyl-tRNA synthetase (ProRS) domain of the prolyl-glutamyl tRNA synthetase (EPRS) during protein translation in an ATP-dependent manner (Keller 2012). In recent years, HF has garnered a lot of attention for its beneficial use as a treatment for a wide variety of diseases including malaria, cancer, fibrosis, and autoimmune diseases (Pines and Spector 2015, Luo 2017).

Halofuginone activates the amino acid response (AAR) program.

During protein synthesis, amino acids, the building blocks of all proteins, are added to tRNAs by aminoacyl tRNA synthetases (aaRS) (Efeyan 2015). There are 20 aminoacyl-tRNA synthetases that are responsible for coupling an amino acid to the 3' terminus of the tRNA molecule (Berg 2002, Ibba 2015). EPRS is a ubiquitously

expressed aaRS that is responsible for binding the amino acids proline or glutamine to their cognate tRNAs during translation (Young 2016). HF binds to the ProRS domain of EPRS and prevents the charging of prolyl-tRNA (Keller 2012). The intracellular accumulation of uncharged tRNAs can result from either the lack of any amino acid or from the inhibition of an aaRS (Kilberg 2005, Efeyan 2015).

Specific to eukaryotes, the accumulation of uncharged tRNAs is the beacon of amino acid deprivation and is sensed by the kinase, general control nonderepressible 2 (GCN2) (Harding 2003, Gallinetti 2013, Pakos-Zebrucka 2016). GCN2 is currently regarded as the sole sensor and effector of the highly conserved eukaryotic nutrient stress response pathway known as the amino acid response (AAR) (Pakos-Zebrucka 2016). Under physiological conditions, the AAR is activated in response to limited amino acid availability and is a part of the mammalian integrated stress response (ISR) (Kilberg 2012, Efeyan 2015, Pakos-Zebrucka 2016). The ISR is an elaborate pro-survival, homeostatic signaling program catalyzed by a collection of four serine/threonine kinases that sense and respond to a variety of microenvironment stress stimuli including heme deprivation, oxidative stress, viral infection, misfolded proteins, UV radiation, proteasome inhibition, and amino acid deficiency (Pakos-Zebrucka 2016). aaRS inhibitors such as HF and HFol function as amino acid-restriction mimetics and have been shown to effectively activate the AAR (Sundrud 2009, Keller 2012).

The AAR response is initiated by the uncharged tRNAs that are produced either by amino acid limitation or by aaRS inhibitors accumulating in the cell and binding two domains of GCN2, the HisRS domain and the C-terminal ribosome binding domain (Dong 2000, Lageix 2015). The binding causes GCN2 to undergo a conformational that

permits its autophosphorylation and subsequent activation of its kinase activity (Dong 2000, Castilho 2014). Activated GCN2 mounts its kinase activity on its downstream target eukaryotic translation initiation factor subunit eIF2α (Gallinetti 2013, Castilho 2014) by phosphorylating serine 51 on eIF2α (Pakos-Zebrucka 2016). All kinases of the ISR converge their activity on the phosphorylation of eIF2α (Pakos-Zebrucka 2016). The phosphorylation of eIF2α inhibits the guanine exchange factor (GEF) activity of the protein eIF2B (Baird and Wek 2012, Kilberg 2012). Under homeostatic conditions, eIF2B facilitates the exchange of eIF2α-GDP for eIF2α-GTP to drive cap-dependent protein translation (Baird 2012). The GTP-bound eIF2α is required for the formation of the methionyl-initiator tRNA ternary complex. The ternary complex, along with other translation initiation factors and the 40S ribosomal subunit, is required to initiate and proceed with cap-dependent translation (Baird 2012). However, when the ISR is activated, the phosphorylation of eIF2α results in a paradox in translation. On one hand, global cap-dependent protein translation is suppressed, but the lack of ternary complex shifts global translation to only translate select mRNAs involved in the adaptation to stress (Barbosa 2013). These mRNAs have upstream open reading frames (uORFs) or internal ribosome entry sites (IRES) that remain efficiently translated even when amino acids are depleted (Hinnebusch 2005, Barbosa 2013).

Activating transcription factor 4 (ATF4) is considered to be the primary activating transcription factor of GCN2 signaling in response to amino acid deprivation (Kilberg 2005, Kilberg 2009). ATF4 forms homodimers and heterodimers with other basic leucine zipper transcription factors and together the complexes facilitate increased transcription of the adaptive genes whose products are involved in amino acid biosynthesis, amino acid

import and feedback regulation to aid in the restoration of homeostasis (Kilberg 2009, Baird and Wek 2012). During the later stages of the GCN2-mediated signaling pathway, eIF2α phosphatases increase their activity and act in concert with each other to dephosphorylate eIF2α as part of the negative feedback loop used to terminate the AAR and resolve the initial stress (Connor 2001, Kilberg 2005, Rei 2016, Pakos-Zebrucka 2016). Normal global protein synthesis and cell function is either restored or the apoptotic program is initiated (Pakos-Zebrucka 2016).

Halofuginone is an effective therapeutic for many pathological tissue remodeling diseases.

HF has been shown to be effective as a potential therapeutic for diseases such as Duchenne Muscular Dystrophy (Huebner 2008), graft-versus-host disease (Nagler 1999, Pines and Nagler 2003), cardiac stress (Qin 2017), chronic lung allograft dysfunction (Oishi 2016), cancer (Elkin 1999), and organ-specific fibrosis (reviewed in Luo 2017). Halofuginone has been shown to be effective at improving functional and structural defects of the heart and improving animal survival in three models of cardiac stress (Qin 2017). In a human cardiomyocyte fibroblast, HF reduced collagen deposition and suppressed the extracellular matrix remodeling characteristic of fibrosis (Qin 2017). In animal models of graft-versus-host disease, pulmonary fibrosis, and pancreatic fibrosis Halofuginone was shown to reduce collagen synthesis (Levi-Schaffer 1996, Pines 2003, Zion 2009). Animal models of Duchenne Muscular Dystrophy have been used to examine the therapeutic action of HF on this disease (Huebner 2008). Halofuginone decreased the levels of collagen and the pro-fibrotic protein, smooth muscle actin (SMA),

and reversed the effects of fibrosis in the respiratory, cardiac and skeletal systems of the affected animals (Huebner 2008).

Our group has shown that HF can hinder the Th17 cell differentiation thereby suppressing Th17-driven inflammation in murine experimental autoimmune encephalomyelitis (Sundrud 2009). We have also shown that at low doses HF suppresses pathogenic inflammation and concomitantly activates the AAR without inhibiting global protein translation (Sundrud 2009, Keller 2012). Interestingly, our group has shown that HF can dampen the transcriptional and translational pro-inflammatory effects of TNFα in an *in vitro* culture of fibroblast-like synoviocytes independent of GCN2 (Kim et. al manuscript in preparation*)*. Although the molecular target is known and the therapeutic relevance of HF is evidenced in the various studies described in the literature (Pines and Nagler 1998, Nanthakumar 2015, Luo 2017), the exact mechanism of action remains unclear.

The current understanding of the mechanism of action of HF as an antifibrotic.

There have been several models proposed over the years as to the mechanism by which HF is able to confer its broad scope of therapeutic benefits on a variety of diseases (Pines and Nagler 1998, Abramovitch 1999, Bruck 2001, McGaha 2002, Turgeman 2008, Roffe 2010, Keller 2012, Shibata 2017). Since HF has been used as an antifibrotic agent in pre-clinical and clinical trials, many of the proposed models have centered around how HF is able to suppress the tissue remodeling program of fibrosis (Pines and Nagler 1998, Roffe 2010, Shibata 2017).

Fibrosis is a pathological condition characterized by the exaggerated and intractable deposition of extracellular matrix (ECM) components that leads to the dysfunction and ultimate failure of the underlying organ or tissue (Wynn 2008, Rockey 2015, Rosenbloom 2017). The excessive ECM deposition during the development of fibrosis is primarily driven by the TGFβ signaling cascade stimulating tissue-resident fibroblasts to upregulate the synthesis of ECM proteins such as collagens, actin, fibronectin, and glycosaminoglycans (Wolters 2014, Meng 2016). TGFβ is a profibrotic growth factor and cytokine that functions as a heterodimer to signals via receptor complexes and activate Smad proteins. Smad proteins are transcriptional activators that when phosphorylated by their respective receptor, translocate to the nucleus and regulate gene expression (Verrecchia 2012, Hata and Chen 2016). One model suggests that HF functions as an antifibrotic by disrupting the TGFβ-signaling cascade through direct inhibition of the phosphorylation of Smad Family Member 3 (Smad3) (Pines and Nagler 1998, Roffe 2010). Our group has proposed a model where the biological effects of HF are due to the direct inhibition of prolyl-tRNA-charging of EPRS (Keller 2012). Collectively, from our initial work in the synoviocytes and the T cells, we hypothesize that HF can elicit its therapeutic effects on a wide breadth of pathogenic tissue remodeling programs and that these effects can be conferred independent of the AAR sensor and effector, GCN2.

The goal of this project was to characterize the transcriptional and translational responses to the HF analog, HFol, in a physiological TGFβ-responsive model using the pulmonary fibroblast cell line, LL29. Additionally, the experiments conducted herein

aimed to illustrate GCN2-independent effects of HFol on a TGFβ-mediated, profibrotic, pathogenic tissue remodeling program in the LL29 cells.

Chapter II.

Methods

Mammalian Cell Culture

All cell lines were cultured at 5% CO_2 at 37°C. US Qualified Fetal Bovine Serum (FBS) was purchased from Life Technologies and manufactured by Gibco.

K4

Transformed human fibroblast-like synoviocytes, K4, provided by Dr. Evelyn Murphy (University College Dublin), were grown in Dulbecco's Modified Eagle Medium (DMEM) (Gibco 11965118) supplemented with 10% fetal bovine serum (FBS) (Gibco), 1mM antibiotics (Penicillin, Streptomycin, Amphotericin B (P/S/A): Lonza 17-745) and 1mM sodium pyruvate (Gibco 11360070).

LL29

Human lung fibroblasts (LL29, AnHa), were purchased from the American Type Culture Collection (ATCC, Manassas, VA). The LL29 cells were originally isolated from a 26-year-old Caucasian female. The cells were cultured in DMEM (Gibco 11965118) supplemented with 10% fetal bovine serum (FBS) (Gibco) and 1mM antibiotics (Penicillin/Streptomycin (P/S): Lonza 17-603) unless otherwise noted.

Chemical inhibitors

HF and HFol were synthesized as described in Keller (2012). HF was reconstituted in 20mM sodium citrate (pH 5.0) to a stock concentration of 10mM. HFol was reconstituted in DMF to a stock concentration of 10mM. Borrelidin was purchased from Adipogen and reconstituted in DMSO to a stock concentration of 10mM. SB431542 was purchased from TOCRIS and reconstituted in DMSO to a stock concentration of 50mM. ISRIB was purchased from Sigma-Aldrich and reconstituted in DMSO to a stock concentration of 2mM. GCN2i was purchased from Axon MedChem and reconstituted in DMSO to a stock concentration of 50mM.

RNA Extraction and Quantitative Real-Time PCR

Prior to harvest, cells were rinsed once with cold 1x Phosphate-buffered saline. Cells were harvested on ice in 400µL Trizol Reagent (Ambion 15596018). RNA was extracted using the Direct-Zol RNA MiniPrep kit (Zymo Research R2060) and eluted in 25µL DNase-free/RNase-free water supplied with the kit. The RNA concentrations were determined using a ND-1000 spectrophotometer (Nanodrop). RNA was reverse-transcribed into cDNAs using the High-Capacity cDNA Reverse Transcription Kit (Ambion 4368814) and diluted as noted in figure legends. Primers were designed against the human genome using the Roche Universal Probe Library System Assay Design tool. Primers were provided by IDT and Sigma Aldrich. Primer sequences and probe sets are included in Table 1. Probes were provided by Roche. Quantitative real-time PCR was performed on a Lightcycler 96 machine (Roche 05815916001) using the Lightcycler 480 Probes Master kit (Roche 04887301001). The thermal conditions were: 95°C for 10 minutes, followed by 45 cycles at 95°C for 10 seconds, 60°C for 30 seconds and 72°C for

1 second and the final step was a cooling period of 30 seconds at 37°C. The fold change expression of each mRNA relative to the untreated control were calculated using the delta-delta CT method (Schmittgen and Livak 2008). GAPDH or PGK1 were used as the endogenous control genes. The specific control gene used is noted in the figure legends. Error bars represent the range of values for the target gene relative to the untreated control. This range is calculated from the ddCT -/+ the standard deviation of the ddCT value (Applied Biosystems).

Table 1: Primer and Probe sets used for qPCR experiments

Gene	Forward Primer	Reverse Primer	Probe #
ACTA2	gcactgccttggtgtgtg	tcccattcccaccatcac	21
ASNS	gatgaacttacgcagggttaca	cgcggagaacatcaaacaa	63
ATF3 (variant 1)	cgtgagtcctcggtgctc	gcctgggtgttgaagcat	1
CHOP	aaggcactgagcgtatcatgt	tgaagatacacttccttcttgaacac	21
COL1A1	ccctctggagcctctggt	gagtccatctttgccaggag	21
CTGF	ctcctgcaggctagagaagc	gatgcacttttgcccttctt	85
CXCL10	gaaagcagttagcaaggaaaggt	gacatatactccatgtagggaagtga	34
GAPDH	agccacatcgctcagacac	gcccaatacgaccaaatcc	60
IDO1	gtgtttcaccaaatccacgat	ctgatagctgggggttgc	20
LAMP3	atttgaccgtctcagatccag	cttgaaggaatgcccgact	9
MMP13	ccagtctccgaggagaaaca	aaaaacagctccgcatcaac	73
PGK1	ggaagcgggtcgttatgag	attgtccaagcagaatttgatg	56
SPARC	ttccctgtacactggcagttc	aatgctccatggggatga	36
TRB3	tccagatcgtgcaactgct	cttcctggacggggtaca	16

Protein Extraction and Western Blot

Following treatments, cells were rinsed with 1X cold PBS. Cells were lysed in 200uL RIPA supplemented with phosphatase and protease inhibitors (Table 2). Cells were scraped in RIPA buffer and incubated on ice for 5 minutes. Lysates were transferred to cold Eppendorf and vortexed briefly. Lysates were then centrifuged at 4°C for 10 minutes at 14000RPM. Supernatant was transferred to new, cold 1.7mL Eppendorf tubes

and quantified by Pierce BCA assay (Thermo Fisher). 3-5µG of the protein lysate was separated on 4-12% gradient Bis-Tris gels (Invitrogen). For wet transfers, gels were transferred to a 0.2µM nitrocellulose membrane (Prometheus) using a wet transfer apparatus for 3 hours at 12 volts. Alternatively, for semi-dry transfers, gels were transferred to 0.2µM nitrocellulose membrane (Bio-Rad) using a semi-dry Trans-Blot Turbo transfer apparatus (Bio-Rad) for 7 minutes at a constant 1.3Å. The membranes were blocked with 5% nonfat milk diluted in 1X Tris-buffered saline with Tween 20 (TBST) for 60 minutes at room temperature then washed three times in 5-minute increments with room temperature TBST before being incubated with primary antibodies (Table 3) overnight at 4°C. After the overnight incubation, membranes were washed three times in 5-minute increments at room temperature with room temperature 1X TBST. The membranes were then incubated with anti-rabbit or anti-mouse IgG conjugated to horseradish peroxidase (Table 3) for 1 hour at room temperature. The membranes were then washed three times in 5-minute increments with room temperature 1X TBST followed by one 10-minute was with room temperature 1X Tris-buffered saline before being developed with enhanced chemiluminescence substrate (Thermo Fisher Scientific: 34075) and imaged on a Pxi Imager (Syngene). Antibody resources and dilutions are included in Table 3.

Table 2: RIPA Lysis Buffer formula

	Final concentration
25x PP1 (1mM Sodium Fluoride; 1mM Sodium Orthovanadate)	1X
500X PP2 (10nM Caliculylin A; 30nM Okadaic Acid)	1X
100mM PMSF	1X (1mM)
100mM N-Ethylmaleimide	1X (1mM)
25X COMPLETE +EDTA (Roche 4693132001)	1X

Table 3: Western Blot Antibodies

	Protein	Catalog Number	Supplier	Dilution
Primary Antibodies				
	ATF4	10835-1-AP	ProteinTech	1:1000
	ACTA2	MS-113-P0	Thermo Fisher	1:800
	COL1A1	GTX112731	Genetex	1:1000
	Cytoplasmic Actin AC40	84700	Sigma	1:5000
	GAPDH	GTX627408	Genetex	1:1000
	GCN1L1	NB100-97851	Novus	1:2000
	LOXL2	GTX105085	Genetex	1:1000
	Phospho-eIF2α	3398	Cell Signaling Technologies	1:1000
	Phospho-GCN2	2425-1	Epitomics	1:1000
	Phospho-Smad2	3108	Cell Signaling Technologies	1:1000
	Phospho-Smad3	9154	Cell Signaling Technologies	1:1000
	Total eIF2α	5324	Cell Signaling Technologies	1:1000
	Total GCN2	3302	Cell Signaling Technologies	1:1000
	Total Smad2	3103	Cell Signaling Technologies	1:1000
	Total Smad3	9513	Cell Signaling Technologies	1:1000
Secondary Antibodies				
	Anti-rabbit IgG, HRP-linked Antibody	7074S	Cell Signaling Technologies	1:3000
	Anti-mouse IgG, HRP-linked Antibody	7076S	Cell Signaling Technologies	1:3000

aaRS transcriptional and translational assays to establish effective dose ranges.

LL29 cells were cultured in DMEM supplemented with 10% FBS and 1mM Penicillin/Streptomycin/Amphotericin B (Lonza 17-745). LL29 cells (p8) were plated into 6-well plates at a 1:4 dilution. 48 hours post plating, media was changed to DMEM

supplemented with 0.2% FBS and 1mM Penicillin/Streptomycin/Amphotericin B (Lonza 17-745) for 24 hours. HFol (800nM) or Borrelidin (4μM) was added to the cells for 6 hours. Cells were harvested for RNA as described above. cDNA was made using 600nG of RNA using the High-Capacity cDNA Reverse Transcription Kit (Ambion 4368814). qPCR was carried out using the protocol described above.

For proline rescue experiments LL29 cells were cultured in DMEM supplemented with 10% FBS and 1mM Penicillin/Streptomycin/Amphotericin B (Lonza 17-745). LL29 cells (p11) were plated into 6-well plates at a 1:4 dilution. Cells were starved in DMEM supplemented with 0.2% FBS supplemented with 1mM Penicillin/ Streptomycin/ Amphotericin B (Lonza 17-745) for 24 hours. Following starvation, cells were treated with 800nM HFol, 4μM Borrelidin, and/or 2mM of the cognate amino acid proline or threonine respectively for 2 hours. Cells were harvested for protein and immunoblotted as described above.

HFol affects TGFβ-induced gene expression and the effects are rescued by the addition of excess proline.

For proline rescue transcriptional assays, LL29 cells were cultured in DMEM (Gibco 11965118) supplemented with 10% fetal bovine serum (Gibco) and 1mM Penicillin/Streptomycin/Amphotericin B (Lonza 17-745). LL29 cells (p11) were plated into 6-well plates at a 1:4 dilution. 48 hours post plating, media was changed to DMEM supplemented with 0.2% FBS and 1mM Penicillin/ Streptomycin/ Amphotericin B (Lonza 17-745) for 24 hours. HF 200nM or 400nM was added to the cells for 6 hours. 2mM of proline was added in conjunction with HF in the applicable samples. Cells were

then treated with TGFβ (Peprotech 100-21) at a final concentration of 10ng/mL for 16 hours. Cells were harvested for RNA using the protocol described above. 400nG cDNA was made using the High-Capacity cDNA Reverse Transcription Kit (Ambion 4368814). qPCR was carried out using the protocol described above. PGK1 was used as the housekeeping gene.

For experiments that assayed gene expression of genes of interest from the transcriptomic data set, LL29 cells (p11) were cultured in 6-well plates in DMEM supplemented with 10% FBS and 1mM Penicillin/Streptomycin (Lonza 17-603). Cells were starved for 24 hours in DMEM supplemented with 0.2% FBS (Gibco) and 1mM P/S (Lonza 17-603). Cells were then treated with 1μM HFol for 6 hours followed by treatment for 24 hours with TGFβ (Peprotech 100-21) at a final concentration of 10ng/mL. Cells were harvested for RNA using the protocol described above. 700nG cDNA was made using the High-Capacity cDNA Reverse Transcription Kit (Ambion 4368814). cDNA was diluted 1:3 and qPCR was carried out using the protocol described above. GAPDH was used as the housekeeping gene.

For experiments that assayed expression levels for proteins of interest from the proteomic data set, LL29 cells (p11) were cultured in 6-well plates in DMEM supplemented with 10% FBS and 1mM Penicillin/Streptomycin (Lonza 17-603). Cells were starved for 24 hours in DMEM supplemented with 0.2% FBS (Gibco) and 1mM P/S (Lonza 17-603). Cells were then treated following the schedule in Table 4 using 1μM HFol and TGFβ (Peprotech 100-21) at a final concentration of 10ng/mL. Total protein lysates were harvested and immunoblotted as described above.

RNA-Seq Analysis

LL29 (P6) were cultured in 10cm plates in DMEM supplemented with 10% FBS and 1mM Penicillin/Streptomycin (Lonza 17-603). Cells were starved for 24 hours in DMEM supplemented with 0.2% FBS (Gibco) and 1mM Penicillin/Streptomycin (Lonza 17-603). Cells were then treated following the timetable described in Table 4. All cells were harvested at the same time. Cells were rinsed with cold 1X Phosphate-buffered saline and then harvested for RNA in 1mL of Trizol Reagent (Ambion 15596018). Total RNA of each sample was qualified for purity on an Agilent Bioanalyzer (RNA Nano service was provided by the Biopolymers Facility at Harvard Medical School). Samples were then sent to the JP Sulzberger Genome Center at the Columbia University Department of Systems Biology (New York) for RNA-Seq analysis using the Illumina HiSeq (Illumina 4000). mRNA was sequenced at a depth of 30 million reads and was mapped to the human genome by the JP Sulzberger Columbia Genome Center at the Columbia University Department of Systems Biology (New York). A parallel experiment was conducted in our lab, and samples were assayed for transcriptional and translational responses consistent with prior findings (data not shown). Raw counts of RNA reads were provided by Columbia Genome Center. Raw count data was input onto the Galaxy web platform (Afgan 2016) and edgeR analysis for differentially expressed genes was carried out.

Total Proteome analysis

LL29 (P6) were cultured in 10cm plates in DMEM supplemented with 10% FBS and 1mM Penicillin/Streptomycin (Lonza 17-603). Cells were starved for 24 hours in DMEM supplemented with 0.2% FBS (Gibco) and 1mM Penicillin/Streptomycin (Lonza

17-603). Cells were then treated following the timetable outlined in Table 4. All cells were harvested at the same time. Cells were rinsed with a cold 1:1 ratio solution of DMEM and PBS. Cells were scraped in 1.5mL of 1X Phosphate-buffered saline. Cells were sent to the Thermo Fisher Scientific Center for Multiplexed Proteomics for Whole Proteome Analysis, Harvard Medical School for quantitative protein identification by Tandem Mass Tag-Mass Spec. A parallel experiment was conducted, and samples were tested for transcriptional and translational responses consistent with prior findings (data not shown). An interaction map of the top 50 upregulated proteins by TGFβ was constructed using STRING v10.5 (Szklarczyk 2017).

Table 4: Outline of the treatment schedule used in the RNA-Seq and Proteomic assays.

Condition	Serum Starvation	HFol	TGFβ	Total experiment time
Control	24 hours DMEM containing 0.2%FBS + P/S	6 hours with DMF	48-hour empty incubation	78 hours
48-hour HFol treatment	24 hours DMEM containing 0.2%FBS + P/S	48 hours with 1.5μM HFol	48-hour empty incubation	120 hours
24-hour HFol treatment	24 hours DMEM containing 0.2%FBS + P/S	24 hours with 1.5μM HFol	48-hour empty incubation	120 hours
HFol and TGFβ	24 hours DMEM containing 0.2%FBS + P/S	6 hours with 1.5μM HFol	48 hours with 10ng/mL TGFβ	78 hours
48 hours TGFβ	24 hours DMEM containing 0.2%FBS + P/S	6 hours with DMF	48 hours with 10ng/mL TGFβ	78 hours

Testing the effect of HFol on SMAD activation in TGFβ-induced LL29 cells.

LL29 cells were cultured in media described above and plated in 6-well plates. Cells were starved for 24 hours in DMEM supplemented with 0.2% FBS (Gibco) and 1mM Penicillin/Streptomycin (Lonza 17-603). Cells were treated with 1μM HFol for 6 hours followed by treatment with SB431542 (TOCRIS) at a final concentration of 10μM for 30 minutes. This was followed by treatment with TGFβ at a final concentration of 10ng/mL for 2 hours. Cells were lysed for total protein using the protein extraction protocol described above and immunoblotted using the protocol described above.

Applying ISRIB to mammalian cells

For K4 experiments cells were cultured in media described above and plated in 6-well plates. K4 cells were starved for 24 hours in DMEM supplemented with 0.2% FBS (Gibco) and 1mM Penicillin/Streptomycin/Amphotericin B (Lonza 17-745). The cells were then treated with 200nM of HF and titrating doses of ISRIB for 4 hours. RNA was extracted according to the protocol described earlier. cDNA was using 1μG of RNA using the High-Capacity cDNA Reverse Transcription Kit (Ambion 4368814). qPCR was carried out using the protocol described above.

For LL29 experiments cells were cultured in media described above and plated in 6-well plates. LL29 cells were starved for 24 hours in DMEM supplemented with 0.2% FBS (Gibco) and 1mM Penicillin/Streptomycin (Lonza 17-603). For immunoblot experiments, cells were serum starved and pretreated with ISRIB for 30 minutes followed by treatment with either 800nM HFol or 4μM Borrelidin. Cells were lysed for total protein using the protein extraction protocol described above and immunoblotted using

the protocol described above. For mRNA expression assays, the cells were serum starved and treated with 1μM of HFol and titrating doses of ISRIB for 6 hours. RNA was extracted according to the protocol described earlier. cDNA was using 450nG of RNA using the High-Capacity cDNA Reverse Transcription Kit (Ambion 4368814). qPCR was carried out using the protocol described above.

Applying GCN2i to mammalian cells

For K4 experiments cells were cultured in media described above and plated in 6-well plates.

K4 cells were treated with 200nM of HF and titrating doses of GCN2i for 4 hours. Cells were lysed for protein and immunoblotted as described above or RNA was extracted, cDNA was made using 750nG of RNA using the High-Capacity cDNA Reverse Transcription Kit (Ambion 4368814). qPCR was carried out using the protocol described above.

K4 cells were also treated with 200nM HF and/or 2μM GCN2i for 16 hours followed by 6 hours of 10ng/mL TNFα. RNA was extracted as described above. cDNA was made using 500nG of RNA using the High-Capacity cDNA Reverse Transcription Kit (Ambion 4368814). qPCR was carried out using the protocol described above.

For LL29 experiments cells (P10) were cultured in media described above and plated in 6-well plates. LL29 cells were treated with 1μM of HFol and varying doses of GCN2i for 4 hours. Cells were lysed for protein and immunoblotted as described above. LL29 cells were also treated in the same manner and RNA was extracted with cDNA

made using 800nG of RNA. cDNA was diluted 1:4 and qPCR was conducted as described above.

Additionally, LL29 cells (p13) were treated with 1μM of HFol and/or 2μM GCN2i for 6 hours followed by 24 hours of 10ng/mL TGFβ. RNA was extracted as described above. cDNA was made using 1uG of RNA using the High-Capacity cDNA Reverse Transcription Kit (Ambion 4368814). cDNA was diluted 1:5 and qPCR was carried out using the protocol described above.

Table 5: List of reagents used

Protocol	Product Name	Manufacturer	Supplier	Item Number
RNA Purification	Direct-zol RNA MiniPrep No TRI-Reagent	Zymo Research	Genesee Scientific	11-331 / R2060
RNA extraction	Trizol	Thermo Fisher Scientific	Fischer Scientific	15596018
cDNA synthesis	High-Capacity cDNA Reverse Transcription Kit	Applied Biosystems	Thermo Fisher Scientific	4368814
Quantitative PCR	LightCycler 480 Probes Master	Roche	Thermo Fisher Scientific	04707494001
Ladder for Westerns	Spectra protein ladder	Thermo Fisher Scientific	VWR	26623
Protein Normalization for Westerns	Pierce BCA protein assay kit	Pierce	Thermo Fisher Scientific	23225
Gels	4-12% Bis-Tris 10 well	Invitrogen	Thermo Fisher Scientific	NW04120
	4-12% Bis-Tris 17 well			NW04127
Transfer of gel	Nitrocellulose membrane	Prometheus	Genesee Scientific	84-875
Semi-Dry Transfer Apparatus	Trans-Blot Turbo Transfer System (Mini)	Bio-Rad Laboratories	Bio-Rad Laboratories	1704150 (system) 1704270 (membrane)
Western Blot Detection	SuperSignal West Dura Extended Duration Substrate	Thermo Fisher Scientific	Thermo Fisher Scientific	34075
Cytokine Treatment	TGFβ	Peprotech	Peprotech	100-21
	TNFα	Gibco	Thermo Fisher Scientific	PHC3015
Inhibitor	SB431542	TOCRIS	TOCIS	1614
	ISRIB	Sigma-Aldrich	Sigma-Aldrich	SML0843
	GCN2i	Axon MedChem	Axon MedChem	A-92

Chapter III.

Results

Determining the effective dosage of Halofuginol to activate the AAR in the human pulmonary fibroblastic cell line, LL29.

Halofuginone (HF) and its less toxic chemical derivative, Halofuginol (HFol) (Figure 1A,1B), have been shown to activate the nutrient sensing amino acid response (AAR) pathway by acting as proline restriction mimetics (Sundrud 2009, Keller 2012). HF has also garnered a lot of attention as an anti-fibrotic in recent years (reviewed in Luo 2017). To further elucidate the mechanism of action of HF family members we decided to assess the transcriptional and translational effects of HFol in the human pulmonary fibroblast cell line, LL29.

First, we needed to establish an effective dose range of HF and HFol in the LL29 cells that would activate the AAR. To do this we treated LL29 cells with HF and HFol at titrating doses for 30 minutes. As described earlier, the AAR signaling cascade is initiated by the phosphorylation of GCN2. We found that the AAR sensor and effector, GCN2, was phosphorylated at a minimum dose of 400nM HF or 500nM HFol (Figure 2A). We next wanted to confirm that the subsequent transcriptional program of the AAR was activated by HF and HFol. To test this, we treated LL29 cells with HFol and another aaRS inhibitor, Borrelidin. Borrelidin, is a threonyl tRNA synthetase inhibitor. By using Borrelidin and HFol, we could consider whether the effects we saw with HFol were unique to HFol inhibiting EPRS or if the effects were shared amongst aaRS inhibitors.

We then decided to look at the transcriptional effects of HFol and Borrelidin. In the LL29 cells treated for 6 hours with 800nM HFol or 4μM Borrelidin both showed transcriptional induction for genes known to be upregulated during amino acid starvation: *asparagine synthesis (ASNS), CCAAT-enhancer-binding protein homologous protein (CHOP), activating transcription factor 3 (ATF3)* and *tribbles homolog 3 (TRB3)* (Jousse 2007, Baird and Wek 2012). HFol showed comparable induction to Borrelidin of *TRB3, ASNS, ATF3* and *CHOP* (Figure 2B-D). Borrelidin showed a stronger induction of ATF3 than HFol (Figure 2E).

Next, we wanted to show that the activation of the AAR by HFol and Borrelidin could be reversed by the addition of excess cognate amino acid, proline or threonine respectively as previously described (Keller 2012). This would demonstrate that HFol and Borrelidin are directly targeting their respective aaRS and the effects we saw were not due to another mechanism. We showed through immunoblot assays, HFol and Borrelidin both induced the phosphorylation of GCN2 and induced the phosphorylation of the GCN2 downstream target, eIF2α (Figure 2F). In the presence of HFol and the cognate amino acid, proline, the levels of phosphorylation of GCN2 and eIF2α were reduced back to basal levels (Figure 2F, lane 4). This result demonstrates that the effects seen with HFol are due specifically to the ability to inhibit prolyl-tRNA charging by EPRS. In the presence of Borrelidin and threonine, the level of phosphorylation of GCN2 was reduced slightly but not to the level of the untreated samples (Figure 2F, lane 5). Additionally, the level of pEIF2α remained unchanged (Figure 2F, lane 6). Cumulatively, these results supported the hypothesis that HFol can activate the AAR in

the fibroblastic cell line, LL29 by competitively inhibiting EPRS binding by proline as these effects are reversed in the presence of excess proline.

Assaying the global effects of Halofuginol on a TGFβ-induced pathogenic tissue remodeling program.

To further characterize the mechanism of action of HFol we were interested in first assaying transcriptional responses already regarded in the field as inducible by TGFβ and to be pro-fibrotic (Wolters 2014). The genes included in our initial experiments were the extracellular matrix components, *smooth muscle actin* (*ACTA2)* and *collagen type 1* (*COL1A1)*. We showed Halofuginone, an analog of HFol, suppressed the gene expression of *ACTA2* and *COL1A1* expression that was induced by TGFβ (Figure 3A, 3B). *ACTA2* was induced 27.2-fold by TGFβ relative to the untreated control (Figure 3A) while *COL1A1* was induced 3.1-fold by TGFβ relative to the untreated control (Figure 3B). The induction of *ACTA2* and *COL1A1* by TGFβ was not affected by the presence of excess proline, but HFol did not significantly suppress this induction when administered in the presence of excess proline (Figure 3A, 3B). This supported the hypothesis that HFol could suppress TGFβ-inducible, profibrotic gene expression and that this suppression was specifically due to the ability of HFol to inhibit prolyl-tRNA charging.

Assaying the response to HFol through global transcriptomic and proteomic profiling

To deepen our understanding of the mechanism of action of HFol, the less cytotoxic analog of HF, in a TGFβ-stimulated LL29 cell, we decided to conduct global transcriptomic and proteomic arrays. This would provide us with a comprehensive list of

genes and proteins that were differentially expressed in LL29 cells upon treatment with HFol in the presence and absence of TGFβ stimulation. It would help us identify additional profibrotic markers that HFol affects that could be used for future therapeutic assays.

From the RNA-Seq data there were 25,559 genes identified (Table 6). There were 1612 genes whose expression was downregulated by HFol compared to the untreated controls (Table 6, row 2). There were 625 genes whose expression was upregulated more than 2-fold by TGFβ (Table 6, row 4). When compared to only TGFβ-stimulated samples, HFol downregulated 733 genes in the presence of TGFβ (Table 6, row 5).

We sorted the RNA-Seq dataset by decreasing log2-fold changes of the ratio of counts between samples only treated with TGFβ and the control, untreated samples and compiled a list of the top 50 genes from this comparison (Table 7). Additionally, for these 50 genes we analyzed the data for the log2 fold changes of the ratio of counts between HFol and TGFβ treated cells compared to samples only treated with TGFβ (Table 7). Unexpectedly, our data only indicated that 4 of the 50 genes upregulated the most by TGFβ were suppressed by HFol in TGFβ-stimulated cells relative to cells only treated with TGFβ (Table 7). The remaining 46 genes either were unchanged in their expression of were upregulated (Table 7).

Several of the top 50 genes upregulated by TGFβ in the LL29 cells have been previously reported to be upregulated by TGFβ in patient-derived pulmonary fibroblasts (Correll 2018). These genes include *cartilage oligomeric matrix protein* (*COMP)*, *actin alpha cardiac muscle I (ACTC1), KN motif and ankyrin repeat domains 4 (KANK4),* and

NADPH oxidase 4 (NOX4) (Correll 2018). From our RNA-Seq data we found that in TGFB-stimulated cells *COMP, NOX4* remained unchanged upon treatment with HFol while *ACTC1* and *KANK4* were upregulated by HFol (Table 8). In addition to *COMP* and *NOX4,* other profibrotic genes, *frizzled class receptor 8 (FZD8)* and *atypical chemokine receptor 7 (CXCR7)* showed transcriptional induction by TGFβ but their expression remained unchanged by HFol (Table 8). While it is still unclear if and how these genes play a role in the pathogenesis of lung fibrosis, their role should be explored further.

Surprisingly, there were several genes we knew from prior data presented in this thesis that were not in the list of the top 50 genes downregulated by HFol in the presence of TGFβ relative to TGFβ-only treated samples including *ACTA2* and *COL1A1*. It was confounding to see in the RNA-Seq data, *ACTA2* was upregulated by HFol 4.4-fold and *COL1A1* was upregulated by HFol 1.3-fold in HFol treated, TGFβ-stimulated cells compared to TGFβ-only treated cells (data not shown).

From the global transcriptomic analysis, we compiled an extensive list of genes found to be regulated by HFol in a TGFβ-induced fibroblast. We chose to explore genes that were significantly modified by HFol in the TGFβ-induced LL29s in the RNA-Seq data. To investigate some of these genes, we treated LL29s with HFol and/or TGFβ for a shorter time course and conducted qPCR on these samples (Figure 5). Some of the genes we were interested in were *ACTA2*, *COL1A1*, *connective tissue growth factor* (*CTGF)*, *secreted protein acidic and cysteine rich* (*SPARC)*, and *lysosomal associated membrane protein 3(LAMP3).* Since we had probed for *ACTA2* and *COL1A1* in a prior experiment (Figure 2A) to initially validate our system, we also probed the new samples for *ACTA2* and *COL1A1* as a control (Figure 5A, 5B). The gene expression of *ACTA2*, *COL1A1* and

extracellular matrix synthesis genes *SPARC* and *CTGF,* all of which are genes implicated in fibrosis, were both induced by TGFβ and suppressed by HFol at the transcriptional level (Figure 5A-D). *LAMP3,* a lysosomal membrane protein (Dominguez-Bautista 2015), was the gene that was the most suppressed by HFol in a TGFβ-stimulated fibroblast relative to a TGFβ-only stimulated fibroblast (Data not shown). In our validation assay *LAMP3* was induced by HFol both in the presence and absence of TGFβ (Figure 5E).

The data obtained from the whole proteome analysis provided us with a list of 7760 proteins (data not shown). Like we did with the RNA-Seq data, we decided to focus our attention to the top 50 proteins whose expression was induced by TGFβ (Table 8). Within this list there were 23 proteins that have been reported in the literature to be implicated in fibrosis (Table 8). Within the top 50 proteins, protein expression was upregulated by TGFβ by a log2 fold change between 1.9 and 5.2 (Table 8). The 10 proteins whose expression was upregulated the most by TGFβ were all suppressed more than 2-fold by HFol (Table 8). Several of the top TGFβ-induced genes from the RNA-Seq data set appeared in the list of the top 50 TGFβ-induced proteins (Table 7, 8). These included: proteoglycan 4 (PRG4), COMP, NOX4, FZD8, insulin-like growth factor-binding protein 3 (IGFBP3), integrin subunit alpha 11 (ITGA11), Hyaluronan And Proteoglycan Link Protein 1 (HAPLN1) and elastin (ELN). The data from the proteomic analysis provided us with insight into other potential candidates whose expression was regulated by HFol. *CTGF* and *SPARC* were both upregulated by TGFβ more than 2-fold on a log2 scale (Table 8 and data not shown). *CTGF* and *SPARC* were both within the top 50 proteins whose expression was suppressed by HFol (Table 8). In order to further

characterize the effects of HFol at the protein level, we decided to generate an interaction map of the top 50 TGFβ-induced proteins (Figure 4). This provided us with a visual representation of the proteins and could help us visualize and extract different pathways or network that HFol may mediate. We identified 13 ECM proteins within the top 50 TGFB-induced protein data set (Table 8, Figure 4: red bubbles).

Many of these down-regulated genes correlated to being downregulated at the protein level. However, there were some genes whose protein levels were downregulated by HFol but whose transcriptional levels remained unchanged (Table 7, 8 and data not shown). Some of these proteins included TPM1, SVEP1, ITGFB8, ADH1B, COL14A1, PPAP2B and KIAA1199 (Table 8). Exploring the role of these proteins could point to additional clues as to the mechanism of action of HFol. Again, we wanted to validate the findings of the global proteomic assay. We assayed total protein lysate from LL29 cells treated on the same time-course as the transcriptomic and proteomic assays (Table 4). We found that COL1A1 was induced in the presence of TGFβ and that this induction was suppressed upon treatment with HFol (Figure 6). Another protein from our proteomic data, whose expression was dampened by HFol was lysyl oxidase like 2 (LOXL2). We showed in our validation assay that LOXL2 protein expression was induced by TGFβ and this induction was suppressed by HFol in the LL29 cells (Figure 6). Additional immunoblot assays were done and validated the proteomic data including ACTA2, CTGF, and SPARC (data not shown). Additional immunoblot assays should be done to validate the other proteins that came out of the proteomic data.

Halofuginol does not inhibit TGFβ-induced SMAD2/3 phosphorylation in LL29 cells.

The ability for HFol to activate the AAR has been shown to be associated with inhibition of pathologic inflammation (Keller 2012). HFol has been investigated and used in the clinic for a variety of diseases discussed in the introduction section. However, the mechanism of action of HF remains unclear.

One model suggests HF confers its antifibrotic, therapeutic effects by disrupting the TGFβ-signaling cascade. Specifically, they suggest that HF inhibits the phosphorylation of SMADS Family Member 3 (Smad3) (Pines and Nagler 1998, Roffe 2010). To test this hypothesis in the fibroblast system I treated LL29 cells with a TGFβ-receptor kinase inhibitor, SB431542 (Figure 1C. SB431542 interferes with TGFβ signaling through inhibition of the TGFβ type 1 receptor kinase, ALK5 (Inman 2002). ALK5 induces phosphorylation of Smad2 and Smad3 (van Caam 2017).

I showed that phosphorylation of Smad2 (Figure 7A, lane 3) and SMAD3 (Figure 7B, lane 3) were both induced in LL29 cells treated with TGFβ. SB431542 was shown to suppress the TGFβ induction of both pSmad2 (Figure 7A, lane 4) and pSmad3 (Figure 7B, lane 5). Interestingly, in the presence of HFol, the TGFβ-induced pSmad2 (Figure 7A, lane 5) and pSmad3 levels (Figure 7B, lane 4) did not change. Through these immunoblot assays I was able to show that HFol does not suppress the TGFβ-induced phosphorylation of Smad2 and Smad3 in the LL29 cells.

Applying the small molecule ISR inhibitor, ISRIB, to investigate the GCN2 independent effects of HF in mammalian cells.

We have established thus far in this project that HFol can activate the AAR in the LL29 fibroblasts and can dampen the TGFβ-induced profibrotic program in the LL29 cells. Another aim of this thesis was to investigate the novel, GCN2-independent uncharged-tRNA sensing pathway identified recently by our lab (Kim et al, manuscript in preparation) in the LL29 fibroblast system. I was interested in examining how HFol affects the programmatic response of a TGFβ-induced fibroblast in a GCN2-independent manner. My initial plan was to generate LL29 cells that were infected with viral particles to knock-down the expression of GCN2 as was done in the K4 cells (Kim et. al manuscript in preparation). However, initial efforts proved unsuccessful. Therefore, I investigated commercially available pharmacological inhibitors that may phenocopy a GCN2 null cell.

Recently an experimental drug, Integrated Stress Response Inhibitor (ISRIB), has been shown to suppress the global ISR program by reversing the peIF2α-mediated translational effects induced by activation of any of the ISR kinases. (Figure 1D, Sidrauski 2015, Zyryanova 2018). We hypothesized that ISRIB could block the induction of the canonical AAR by HFol and we could then investigate the therapeutic effects of HFol that are independent of the AAR.

To test this hypothesis, we tested various doses of ISRIB on K4 synoviocytes, the system where our group first identified and characterized the GCN2-independent effects of HF. First, we attempted to establish a dose of ISRIB that was able to reverse the activation of the AAR by HF in the K4 synoviocytes. Since the phosphorylation of eIF2α

shifts translation from being CAP-dependent to uORF mediated, we wanted to see if ISRIB reversed the effects of HF at the translational level. We treated K4 synoviocytes with 800uM of HFol and titrating doses of ISIRB ranging from 1μM to 2μM. We found that HF induced transcription of ATF4-regulated, AAR genes *TRB3* and *ASNS* (Figure 8A). ISRIB did reduce the mRNA levels by 2-fold, but it did not reduce them to the levels of the untreated control (Figure 8A). We then thought the preincubation time with ISRIB could perhaps affect its ability to suppress the AAR activation by HF. We treated K4 synoviocytes with ISRIB for 0 minutes, 30 minutes or 60 minutes prior to HF treatment. Again, we found that ISRIB could not suppress the HF-mediated transcriptional induction of *TRB3* or *ASNS* (Figure 8B).

Since this thesis focused on the effects of HFol in the LL29 cells we decided to see if ISRIB could suppress the transcriptional and translational effects of HFol in these cells. First, we showed HFol and Borrelidin induced the phosphorylation of eIF2α (Figure 9A). But again, none of the doses of ISRIB reversed the pEIF2α levels back to baseline (Figure 9A). We decided to test if ISRIB could reverse the transcriptional effects of HFol. We tested various doses of ISRIB in LL29 cells that had been treated with HFol. The transcriptional induction of *ASNS* and *TRB3* was evident with HFol, but again ISRIB only suppressed these levels slightly and not to the levels of the untreated control samples (Figure 9B).

Applying a GCN2 kinase inhibitor to investigate GCN2-independent signaling by HF.

As ISRIB could not successfully reverse the HF-mediated phosphorylation of eIF2α, we wanted to try to block the activation of GCN2 by HF. GCN2i is an ATP-

competitive inhibitor that selectively inhibits the kinase activity of GCN2 (Figure 1E, Nakamura 2018). GCN2i was shown in acute lymphoblastic leukemia cells to suppress the phosphorylation of eIF2α by GCN2 and the subsequent downstream adaptive translational response orchestrated by GCN2 upon amino acid depletion (Nakamura 2018). GCN2i has been shown to phenocopy the transcriptional and translational responses of a GCN2-knockout mouse embryonic fibroblast (MEF) (Nakamura 2018). It was possible GCN2i could provide us with a tool to begin elucidating GCN2-independent translational effects of HFol in a TGFβ-responsive fibroblast.

To start, I wanted to ask if GCN2i could recapitulate the previous finding of a GCN2-independent gene regulation program elicited by HF in the K4 synoviocytes (Kim et al, manuscript in preparation). In K4 GCN2-knockdown synoviocytes, HF was shown to dampen a TNFα-induced tissue remodeling program (Kim et al, manuscript in preparation). In K4 synoviocytes I found that 2μM of GCN2i inhibited HF-induced phosphorylation of eIF2α and reduced the phosphorylation of GCN2 (Figure 10A). At the transcriptional level, HF induced ATF4 regulated genes, *ASNS* and *TRB3* (Figure 10B). This transcriptional induction was suppressed when 2μM of GCN2i was added in conjunction with HF (Figure 10B). This indicated GCN2i application counteracted the activation of the AAR by HF, mimicking a GCN2-null cell. To further validate the GCN2i system, we wanted to confirm the GCN2-independent effects of HF on a TNFα-stimulated inflammatory response in K4 synoviocytes (Kim et al manuscript in preparation). The mRNA expression of the pro-inflammatory cytokine *CXLC10*, the matrix metalloproteinase *MMP13* and the immunoregulatory enzyme *IDO1*, genes implicated in the pathogenies of rheumatoid arthritis, was measured by qPCR. The gene

expression was shown to be induced by TNFα and this induction was suppressed by HF (Figure 11A). Importantly, HF was shown to continue to suppress the TNFα-induced gene expression of *IDO1, MMP13* and *CXCL10*, in the presence of GCN2i (Figure 11A). These experiments established GCN2i was able to phenocopy the results we saw in the GCN2-knockdown K4 cells (Kim et al, manuscript in preparation). Therefore, we decided to apply GCN2i to the LL29 cells as a way to investigate GCN2-independent effects without having to generate knockdown or knockout LL29 cells.

First, I established the dosage at which GCN2i inhibited the HFol-induced phosphorylation of eIF2α in the LL29 cells that is characteristic of an activated AAR response (Figure 12A). Next, I established that the same dosage of GCN2i, 2μM, also dampened the translational induction ATF4-regulated genes, *ASNS* and *TRB3* in the LL29 cells (Figure 12B). While the inhibition of pGCN2 by GCN2i did not track with the decrease in the pEIF2α levels and the decrease of ATF4-mediated translational response, it is possible that the autophosphorylation of GCN2 was still occurring even if the activity was suppressed. This should be explored further to better understand the discordance in this data.

After showing successful blockage of HF-induced, GCN2-mediated transcriptional and translational responses, I decided to apply GCN2i in combination with HFol to TGFβ-stimulated LL29 cells to investigate the GCN2-independent effects of HFol on the TGFβ-mediated, profibrotic response. I decided to first assess the GCN2-independent transcriptional effects of HFol on genes shown previously in this thesis to be induced by TGFβ and suppressed by HFol. I conducted qPCR on TGFβ-stimulated LL29 cells that had been treated with 1μM of HFol and 2μM of GCN2i. The gene expression

levels of *COL1A1, ACTA2*, *SPARC* and *CTGF* were measured by qPCR (Figure 13A-D). In TGFβ-stimulated LL29s, the expression of these genes was induced relative to untreated controls (Figure 13A-D). HFol treated, TGFβ-stimulated cells showed weakened induction of gene expression relative to untreated controls. Interestingly, treatment with GCN2i resulted in a greater induction of *ACTA2, SPARC,* and *COL1A1* in the TGFβ-stimulated cells relative to the samples only treated with TGFβ (Figure 13A-C). The profibrotic gene expression of *ACTA2* and *SPARC* were inhibited similarly in TGFβ-stimulated cells treated with GCN2i and HFol as TGFβ-stimulated cells treated with only HFol (Figure 13A, 13C). *CTGF* showed a reduced transcriptional induction by TGFβ in the presence of GCN2i and there was not a strong inhibitory effect of HFol in those samples (Figure 13D). Cumulatively, this data supports the working model that Halofuginol functions as an EPRS inhibitor to activate the canonical AAR as well as suppress the TGFβ-induced profibrotic tissue remodeling program independent of GCN2 in the LL29 fibroblasts (Figure 14).

Figures and Tables

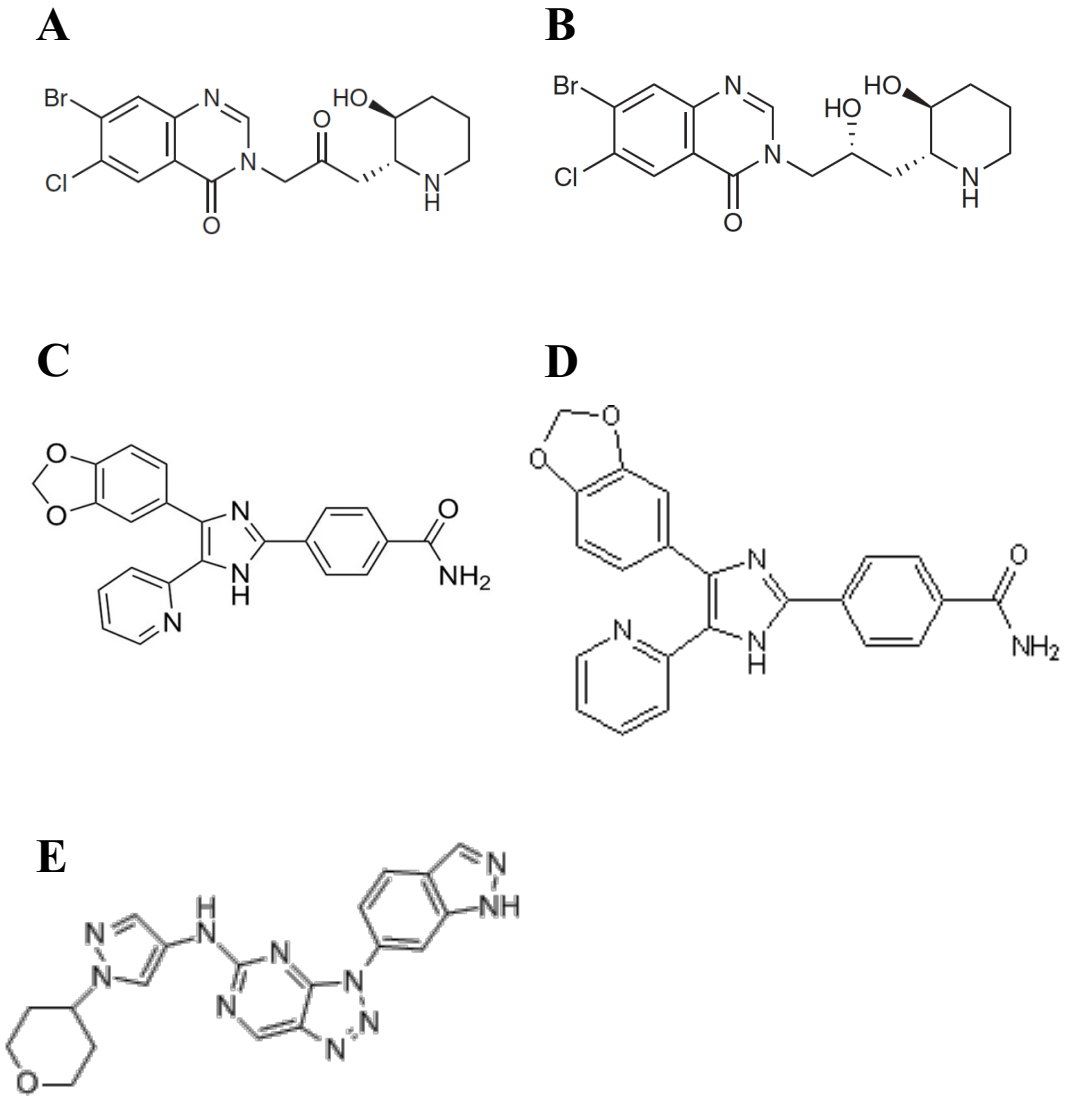

Figure 1: Chemical structures of the various inhibitors used in the LL29 lung fibroblasts.

(A) Halofuginone (Keller 2012). (B) Halofuginol (Keller 2012). (C) SB431542 (TOCRIS). (D) ISRIB (Sigma Aldrich). (E) GCN2i (Axon MedChem).

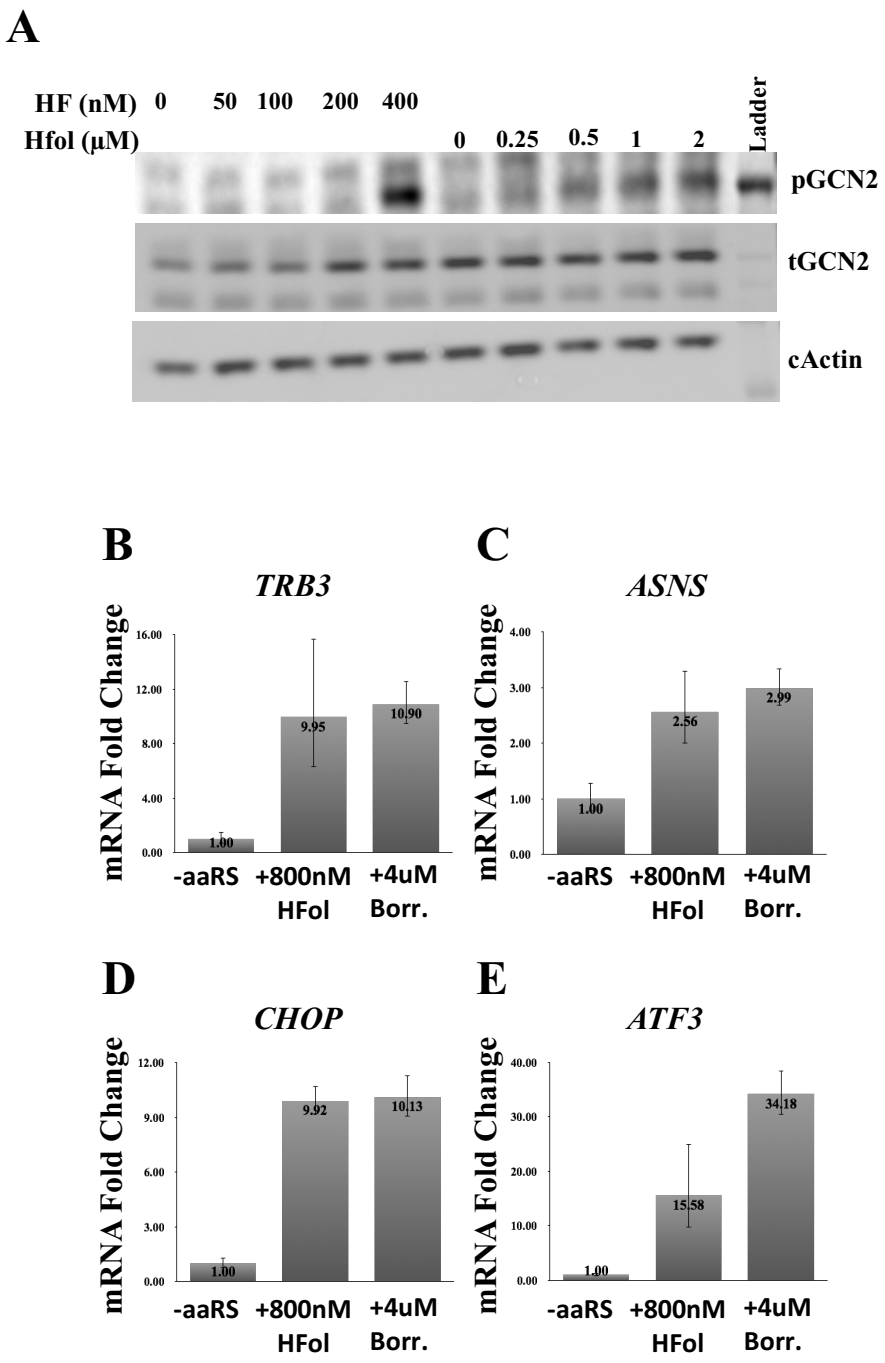
A
HF (nM) 0 50 100 200 400
Hfol (μM) 0 0.25 0.5 1 2 Ladder
pGCN2
tGCN2
cActin
B
TRB3
mRNA Fold Change
16.00
12.00
8.00
4.00
0.00
1.00
9.95
10.90
-aaRS
+800nM HFol
+4uM Borr.
C
ASNS
mRNA Fold Change
4.00
3.00
2.00
1.00
0.00
1.00
2.56
2.99
-aaRS
+800nM HFol
+4uM Borr.
D
CHOP
mRNA Fold Change
12.00
9.00
6.00
3.00
0.00
1.00
9.92
10.13
-aaRS
+800nM HFol
+4uM Borr.
E
ATF3
mRNA Fold Change
40.00
30.00
20.00
10.00
0.00
1.00
15.58
34.18
-aaRS
+800nM HFol
+4uM Borr.

F

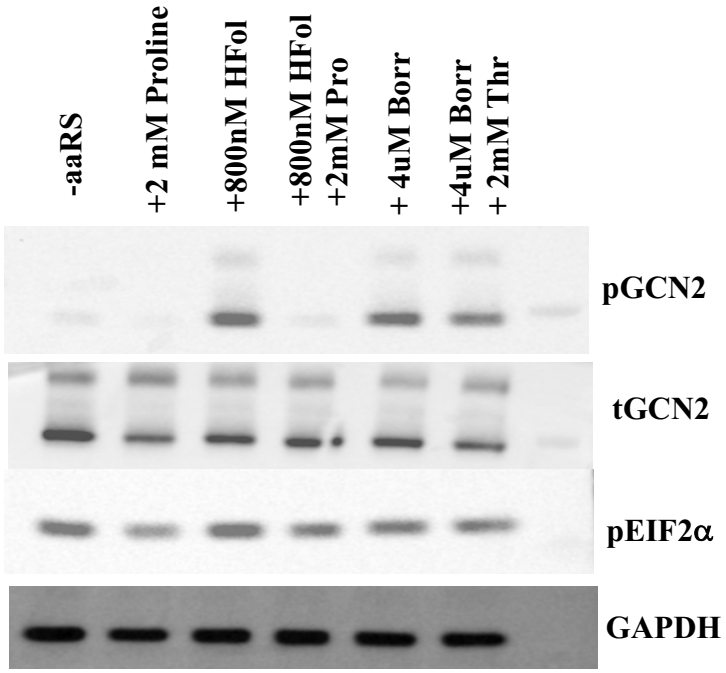

Figure 2: Comparing the dose response of HFol in the LL29 lung fibroblast.

(A) After a 24-hour serum starvation, LL29 cells were treated with HF or HFol for 30 minutes and protein extracts were immunoblotted for phospho-GCN2 and total GCN2. Cytoplasmic actin was used as the loading control. (B-D) LL29 cells were starved for 24 hours in low-serum media followed by treatment with an aaRS inhibitor (800nM HFol or 4μM Borrelidin) for 6 hours. Fold change expression of (B)TRB3, (C)ASNS, (D)CHOP and (E)ATF3 were measured by qPCR relative to untreated control. GAPDH was the housekeeping gene. Results are representative of three independent experiments. (F) LL29 cells were starved for 24 hours followed by a 2-hour treatment with 800nM HFol, 4μM Borrelidin and/or 2mM of their competitive amino acid. Protein extracts were immunoblotted for phospho-GCN2, total GCN2 and phospho-eIF2α. GAPDH was used as the protein loading control.

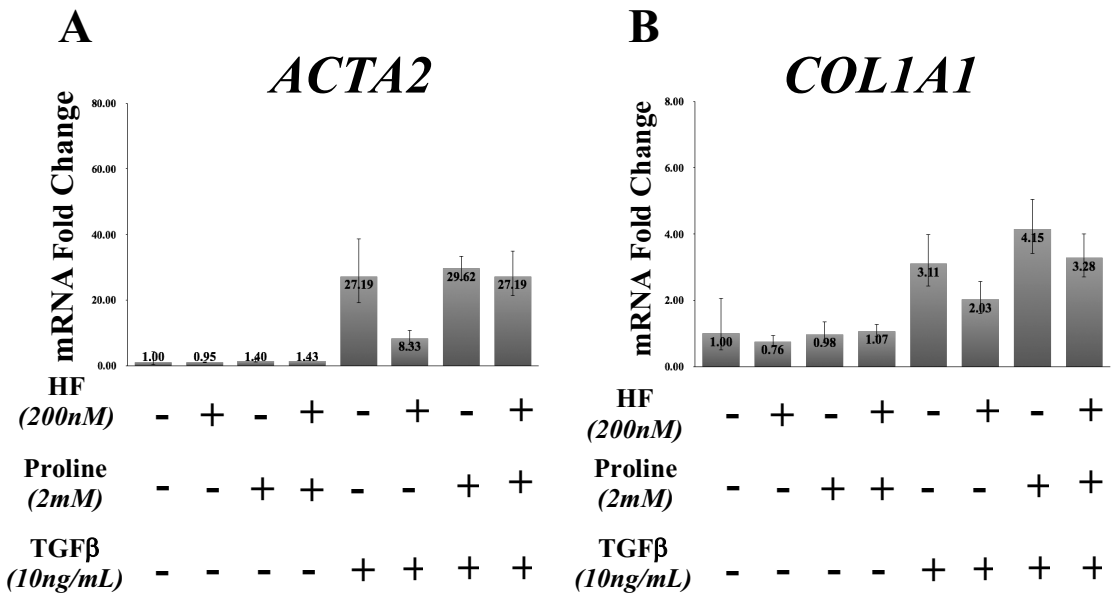

Figure 3: Assaying the transcriptional effects of HFol to the TGFβ-induced program in the LL29 lung fibroblast.

LL29 cells treated with 200nM HF in the presence or absence of 2mM proline for 6 hours followed by 16-hour treatment with TGFβ at a final concentration of 10ng/mL. Fold change expression of (A) SMA and (B) COL1A1 were measured relative to untreated control. PGK1 was the housekeeping gene. Results are representative of three independent experiments

Table 6: Differential expression counts from the RNA-Seq data.

Table indicating the differential expression counts of upregulated, unchanged (flat) and downregulated genes from the RNA-Seq data with a minimum Log2 fold change greater than 2. Differential Expression Count table was generated using Galaxy Web Platform (Liu et al. 2015)

Comparison	Up-regulated	Flat	Down-regulated
Cells treated with HFol for 48 hours compared to the untreated control cells	456	23836	1267
Cells treated with HFol for 24 hours compared to the untreated control cells	451	23496	1612
Cells treated with HFol for 6 hours and TGFβ for 48 compared to the untreated control cells	776	22822	1901
Cells treated with TGFβ for 48 hours compared to the untreated control cells	625	23673	1261
Cells treated with HFol for 6 hours and TGFβ for 48 compared to cells treated with TGFβ for 48 hours	456	24370	733

Table 7: Top 50 genes whose expression is upregulated by TGFβ relative to control cells from total cell RNA-Seq.

Genes are organized in order of decreasing log2 fold change ratio of the sum of the mRNA counts of the two biological replicates of TGFβ and the sum of the biological replicates of Control (log2(TGFβ/Control)). The log2 ratios of the gene counts of the cells treated with HFol and TGFβ and the sum of counts of the biological replicates of the cells treated with only TGFβ (log2(Hfol,TGFB/TGFB)) are presented. Highlighted rows represent genes identified in the literature to have a potential role in the pathogenesis of fibrosis.

	Gene Symbol	**Description**	**Log2 fold change (Ratio) TGFβ /Control**	**Log2 fold change (Ratio) of HFol,TGFβ / TGFβ**	**Citation**
1	PRG4	Proteoglycan 4	10.237	2.206	
2	COMP	Cartilage oligomeric matrix protein	8.950	0.469	Schulz 2016
3	KANK4	KN Motif And Ankyrin Repeat Domains 4	8.751	1.890	
4	ADAMTS16	ADAM Metallopeptidase With Thrombospondin Type 1 Motif 16	8.623	2.628	Bergmeier 2018
5	ST6GAL2	ST6 Beta-Galactoside Alpha-2,6-Sialyltransferase 2	8.607	2.966	
6	ISLR2	Immunoglobulin Superfamily Containing Leucine Rich Repeat 2	8.392	3.534	
7	PADI2	Peptidyl Arginine Deiminase 2	8.111	3.981	
8	KCNH1	Potassium Voltage-Gated Channel Subfamily H Member 1	7.929	-0.988	
9	ITGA11	Integrin Subunit Alpha 11	7.365	1.206	Bansal 2017
10	MDFI	MyoD Family Inhibitor	7.207	1.030	

	Gene Symbol	Description	Log2 fold change (Ratio) TGFβ /Control	Log2 fold change (Ratio) of HFol, TGFβ / TGFβ	Citation
11	SLCO2A1	Solute Carrier Organic Anion Transporter Family Member 2A1	7.100	0.668	
12	IGFBP3	Insulin Like Growth Factor Binding Protein 3	6.887	2.464	Pilewski 2005
13	NOX4	NADPH oxidase 4	6.876	0.477	Hotta 2018
14	MYOZ1	Myozenin 1	6.772	4.343	
15	PLN	Phospholamban	6.765	5.956	
16	FOXS1	Forkhead Box S1	6.736	2.299	
17	LOC100507378	Uncharacterized	6.728	1.173	
18	PI16	Peptidase Inhibitor 16	6.709	1.917	
19	KRT18	Keratin 18	6.392	1.851	
20	ACTBL2	Actin, Beta Like 2	6.254	3.921	
21	CXCR7	C-X-C Motif Chemokine Receptor 7	6.244	-0.116	Cully 2016
22	INHBE	Inhibin Subunit Beta E	6.158	2.446	
23	ANKRD1	Ankyrin Repeat Domain 1	6.134	6.379	
24	DYSF	Dysferlin	6.096	2.135	Demonbreun 2016
25	C18orf1	Low Density Lipoprotein Receptor Class A Domain Containing 4	6.093	0.816	
26	TSPAN2	Tetraspanin 2	6.079	2.041	
27	CES1	Carboxylesterase 1	6.078	5.670	
28	TM7SF4	Dendrocyte Expressed Seven Transmembrane Protein	6.063	3.276	
29	ACTC1	Actin, Alpha, Cardiac Muscle 1	6.003	4.950	
30	FZD8	Frizzled-8	5.996	0.226	Spanjer 2016

	Gene Symbol	Description	Log2 fold change (Ratio) TGFβ /Control	Log2 fold change (Ratio) of HFol, TGFβ / TGFβ	Citation
31	C5orf46	Chromosome 5 Open Reading Frame 46	5.979	2.643	
32	SYTL5	Synaptotagmin Like 5	5.958	3.425	
33	VAV3	Vav Guanine Nucleotide Exchange Factor 3	5.929	5.021	
34	KCNMB1	Potassium Calcium-Activated Channel Subfamily M Regulatory Beta Subunit 1	5.918	5.396	
35	HAPLN1	Hyaluronan And Proteoglycan Link Protein 1	5.856	3.067	
36	LOC283731	Uncharacterized	5.732	-0.344	
37	LOC283875	Uncharacterized	5.728	0.968	
38	AMTN	Amelotin	5.705	-2.924	Nakayama 2018
39	HSD17B6	Hydroxysteroid 17-Beta Dehydrogenase 6	5.668	4.312	
40	NINJ2	Ninjurin 2	5.655	1.894	
41	ELN	Elastin	5.652	2.949	
42	HBEGF	Heparin Binding EGF Like Growth Factor	5.628	-0.311	
43	SCRG1	Stimulator Of Chondrogenesis 1	5.606	5.235	
44	DKK2	Dickkopf WNT Signaling Pathway Inhibitor 2	5.569	3.447	
45	LOC100507263	Uncharacterized	5.556	2.396	
46	SLC7A4	Solute Carrier Family 7 Member 4	5.539	0.377	
47	SYT12	Synaptotagmin 12	5.502	2.401	

	Gene Symbol	Description	Log2 fold change (Ratio) TGFβ /Control	Log2 fold change (Ratio) of HFol, TGFβ / TGFβ	Citation
48	PIK3AP1	Phosphoinositide -3-Kinase Adaptor Protein 1	5.476	3.080	
49	OPCML	Opioid Binding Protein/Cell Adhesion Molecule Like	5.454	-1.043	
50	ROS1	ROS Proto-Oncogene 1, Receptor Tyrosine Kinase	5.362	0.660	

Table 8: Top 50 proteins whose expression is upregulated by TGFβ relative to control cells from global proteomic analysis.

Proteins are organized in order of decreasing log2 fold change ratio of the average scaled data counts between TGFβ stimulated cells and the control samples. Log2 ratios of the HFol and TGFβ stimulated samples and the TGFβ stimulated samples are shown in the neighboring column. Data is representative of two independent experiments. Highlighted rows indicate proteins identified in the literature to be involved in the pathogenesis of fibrosis.

	Gene Symbol	**Description**	**Quantified Spectral Counts**	**Log2(Ratio) TGFβ/Control**	**Log2(Ratio) of HFol, TGFβ / TGFβ**	**Citation**
1	PRG4	Proteoglycan 4	1	5.20	-4.22	
2	TSPAN2	Tetraspanin-2	1	4.85	-4.60	
3	IGFBP3	Isoform 2 of Insulin-like growth factor-binding protein 3	13	4.47	-4.53	Pilewski 2005
4	ELN	Isoform 4 of Elastin	5	4.41	-4.91	
5	SEMA7A	Semaphorin-7A	44	4.31	-4.53	De Minicis 2013
6	ELN	Isoform 8 of Elastin	1	4.29	-4.53	
7	ARHGEF26	Rho guanine nucleotide exchange factor 26	1	4.22	-3.90	
8	FZD8	Frizzled-8	3	4.12	-2.76	Spanjer 2016
9	AMIGO2	Amphoterin-induced protein 2	8	3.88	-2.06	
10	ADAM12	Disintegrin and metalloproteinase domain-containing protein 12	7	3.78	-3.79	Cipriani 2016
11	HBEGF	Proheparin-binding EGF-like growth factor	1	3.74	-0.51	
12	ITGA11	Isoform 2 of Integrin alpha-11	13	3.51	-3.56	Bansal 2017
13	COMP	Cartilage oligomeric matrix protein	1	3.24	-2.50	Schulz 2016

	Gene Symbol	Description	Quantified Spectral Counts	Log2(Ratio) TGFβ/Control	Log2(Ratio) of HFol, TGFβ / TGFβ	Citation
14	LRRC32	Leucine-rich repeat-containing protein 32	4	3.10	-3.80	
15	HAPLN1	Hyaluronan and proteoglycan link protein 1	1	3.09	-3.30	
16	PMEPA1	Transmembrane prostate androgen-induced protein	1	3.07	-1.44	
17	REV3L	DNA polymerase zeta catalytic subunit	3	3.02	-2.56	
18	TGFB1	Transforming growth factor beta-1	9	2.90	-2.61	
19	FSTL3	Follistatin-related protein 3	1	2.71	-1.82	
20	CTGF	Connective tissue growth factor	35	2.70	-4.85	Lipson 2012
21	PCDH10	Protocadherin-10	12	2.68	-2.21	
22	PCDH1	Isoform 2 of Protocadherin-1	4	2.65	-1.58	
23	UNC5B	Netrin receptor UNC5B	15	2.60	-2.42	
24	COL4A1	Collagen alpha-1 (IV) chain	9	2.56	-3.23	Zeng 2016
25	ITIH2	Inter-alpha-trypsin inhibitor heavy chain H2	8	2.56	-1.74	
26	TPM1	Isoform 10 of Tropomyosin alpha-1 chain	26	2.32	0.50	Otogawa 2009
27	TNFAIP6	Tumor necrosis factor-inducible gene 6 protein	1	2.31	-1.70	
28	IL11	Interleukin-11	1	2.30	0.78	Schafer 2017
29	XYLT1	Xylosyltransferase 1	16	2.29	-2.07	
30	FAM101B	Protein FAM101B	3	2.28	-1.79	

	Gene Symbol	Description	Quantified Spectral Counts	Log2(Ratio) TGFβ/Control	Log2(Ratio) of HFol, TGFβ / TGFβ	Citation
31	IGFBP7	Insulin-like growth factor-binding protein 7	14	2.25	-4.23	
32	SERPINE1	Plasminogen activator inhibitor 1	38	2.24	-1.48	Samarakoon 2013
33	NOX4	NADPH oxidase 4	1	2.23	-1.42	Samarakoon 2013
34	AQP1	Aquaporin-1	2	2.21	-3.21	Galán-Cobo 2018
35	VCAN	Versican core protein	34	2.18	-3.19	
36	COL7A1	Collagen alpha-1 (VII) chain	11	2.18	-2.79	
37	VCAN	Isoform V1 of Versican core protein	1	2.14	-3.17	
38	KIAA1324	UPF0577 protein KIAA1324	1	2.12	-3.15	
39	TIMP3	Metalloproteinase inhibitor 3	15	2.11	-3.75	Selman 2000
40	COL5A1	Collagen alpha-1(V) chain (Fragment)	3	2.11	-4.67	Lei 2016
41	INHBA	Inhibin beta A chain 2	7	2.10	-2.24	
42	SERPINE2	Glia-derived nexin	1	2.10	-1.94	Li 2016
43	ITGBL1	Integrin beta-like protein 1	12	2.07	-3.02	Wang 2017
44	ANKH	Progressive ankylosis protein homolog	3	2.06	-2.53	
45	TPM1	Isoform 3 of Tropomyosin alpha-1 chain	18	2.04	-0.07	Otogawa 2009
46	SLC6A6	Sodium- and chloride-dependent taurine transporter	4	2.03	-2.22	
47	FN1	Ugl-Y3 (Fragment)	1	2.02	-3.70	
48	SPOCK1	Testican-1	7	1.98	-2.80	
49	CDH2	Cadherin-2	18	1.96	-1.72	Black 2018

	Gene Symbol	Description	Quantified Spectral Counts	Log2(Ratio) TGFβ/Control	Log2(Ratio) of HFol, TGFβ / TGFβ	Citation
50	SERPINE2	Isoform 3 of Glia-derived nexin	17	1.91	-2.15	Li 2016

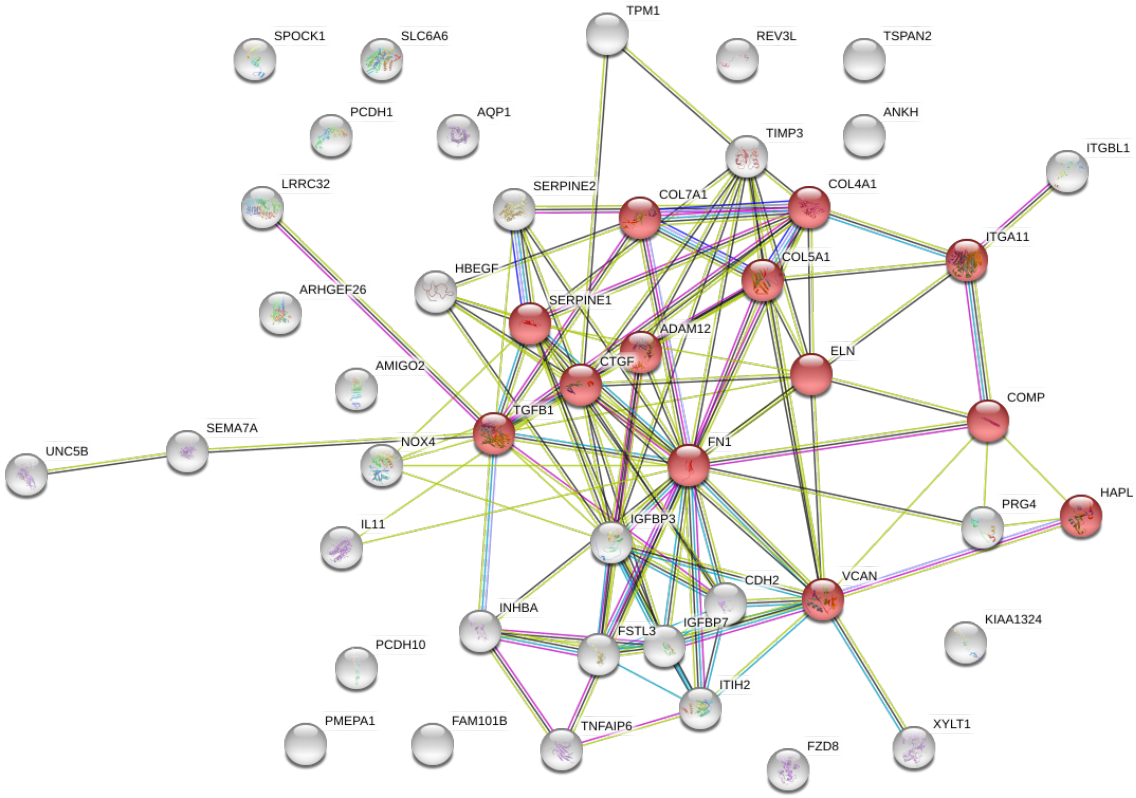

Figure 4: Network map of top 50 proteins in a TGFβ-induced LL29 fibroblast

Interaction map (String v. 10.5) illustrating the top 50 proteins upregulated by TGFβ in LL29 cells treated with TGFβ for 48 hours relative to untreated, control LL29 cells (Table 8). Minimum required interaction score was set to the medium confidence of 0.400. Red highlighted proteins indicate those involved in the extracellular matrix organization.

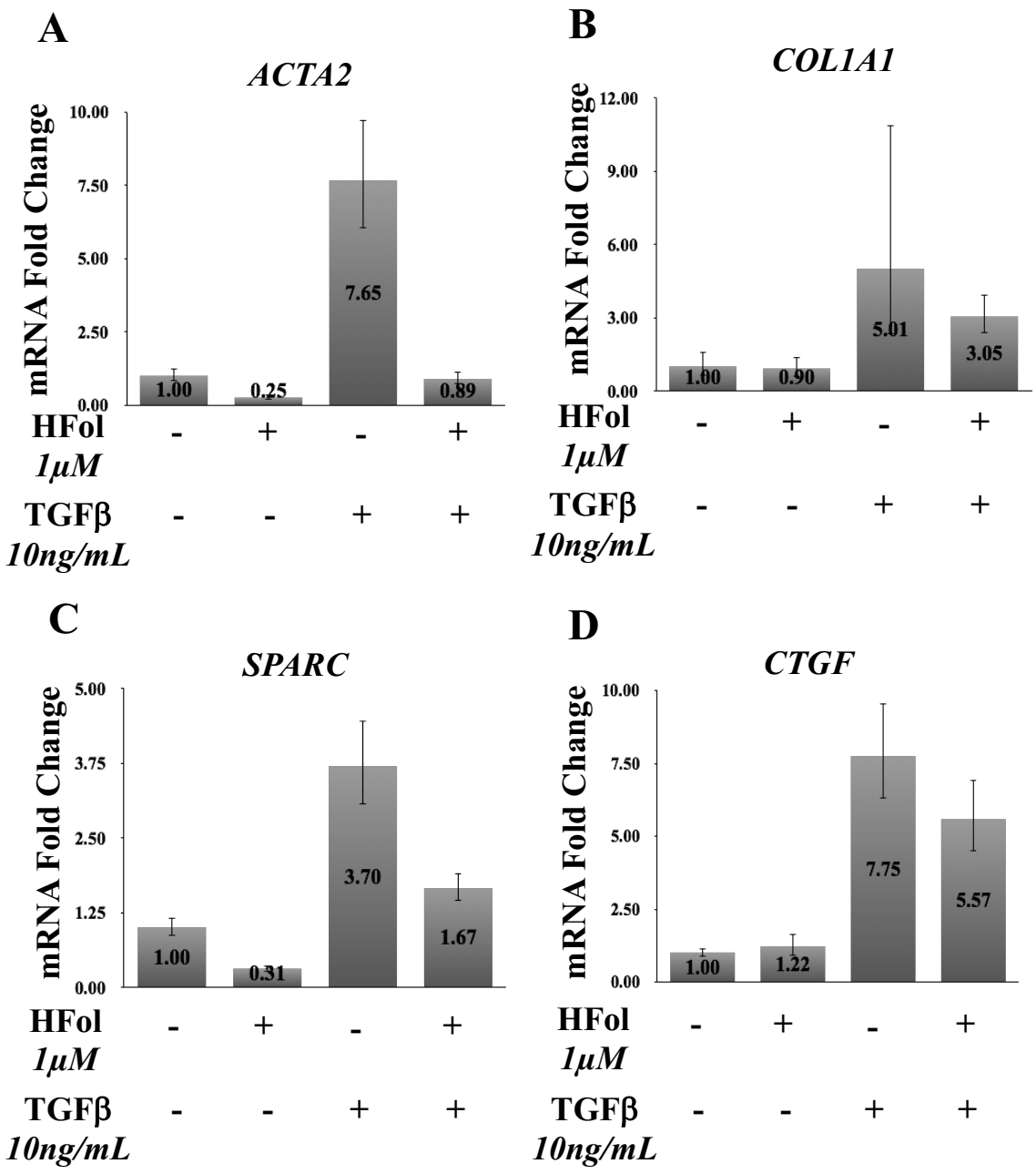
A
ACTA2
mRNA Fold Change
10.00
7.50
5.00
2.50
0.00
1.00
0.25
7.65
0.89
HFol 1μM
TGFβ 10ng/mL
- + - +
- - + +
B
COL1A1
mRNA Fold Change
12.00
9.00
6.00
3.00
0.00
1.00
0.90
5.01
3.05
HFol 1μM
TGFβ 10ng/mL
- + - +
- - + +
C
SPARC
mRNA Fold Change
5.00
3.75
2.50
1.25
0.00
1.00
0.31
3.70
1.67
HFol 1μM
TGFβ 10ng/mL
- + - +
- - + +
D
CTGF
mRNA Fold Change
10.00
7.50
5.00
2.50
0.00
1.00
1.22
7.75
5.57
HFol 1μM
TGFβ 10ng/mL
- + - +
- - + +

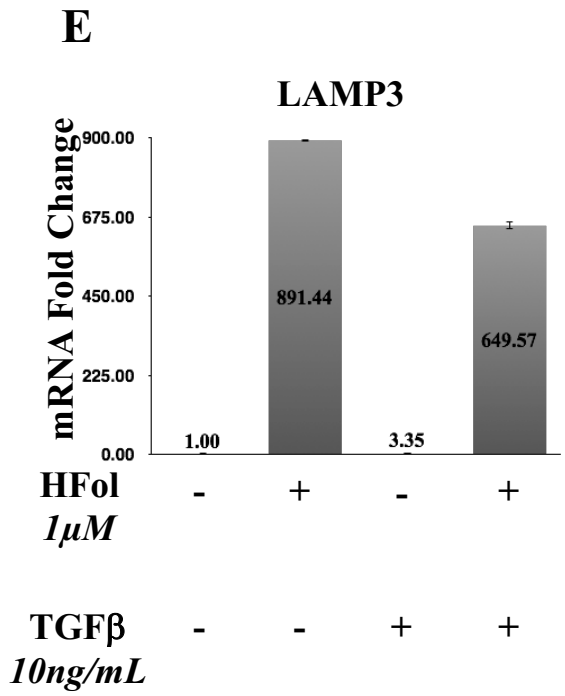

Figure 5: Assaying genes of interest from the RNA-Seq analysis.

qPCR was conducted on RNA isolated from LL29 cells that were serum starved and then treated with 1μM HFol for 6 hours and/or 10ng/mL TGFβ for 24 hours. The mRNA fold change expression of (A) ACTA2, (B) COL1A1, (C) SPARC, (D) CTGF, and (E) LAMP3 for each treatment condition relative to untreated control samples are displayed. GAPDH was used as the housekeeping gene. Results are representative of three independent experiments.

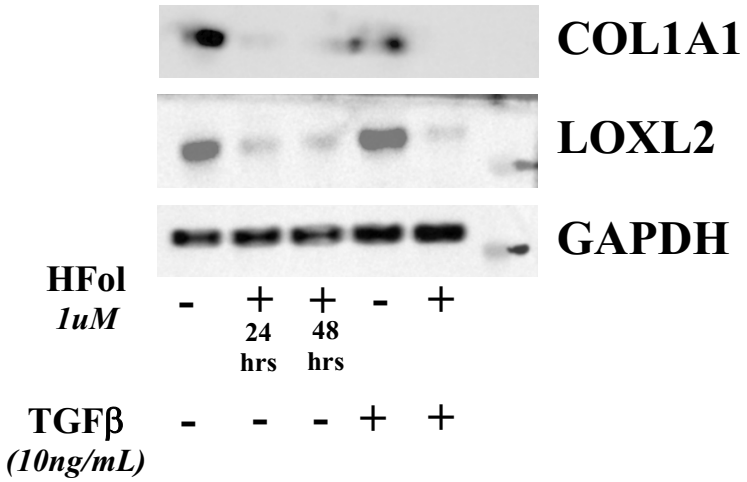

Figure 6: Assaying proteins of interest from the global proteomic data analysis.

After a 24-hour serum starvation, LL29 cells were treated with 1μM HFol and/or 10ng/mL TGFβ according to the schedule outlined in Table 4. Protein extracts were immunoblotted for COL1A1 and LOXL2. GAPDH was used as the protein loading control

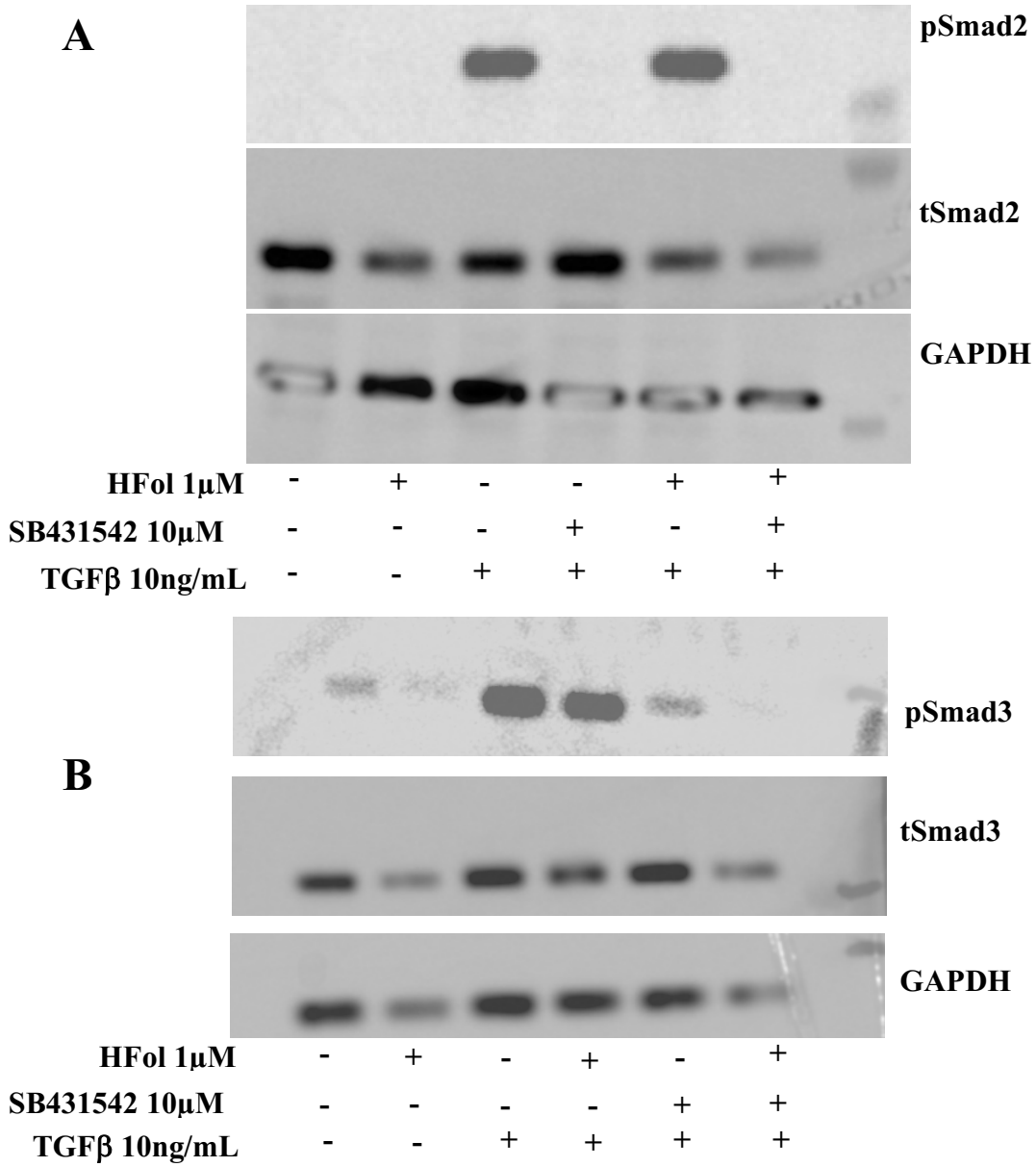

Figure 7: Comparing the translational effects of HFol and a TGFβ-receptor kinase inhibitor on the phosphorylation of Smad2 and Smad3 in the LL29 lung fibroblast.

LL29 cells were serum starved in 0.2% FBS DMEM for 24 hours prior to treatment. Cells were treated with 1µM HFol for 6 hours followed by 10µM SB431542 for 30 minutes. This was followed by treatment with TGFβ at a final concentration of 10ng/mL for 2 hours. 5µG of total protein extract was immunoblotted for (A) phospho-Smad2 and total-Smad2 or (B) phospho-Smad3 and total-Smad3. GAPDH was used as the loading control for both immunoblots.

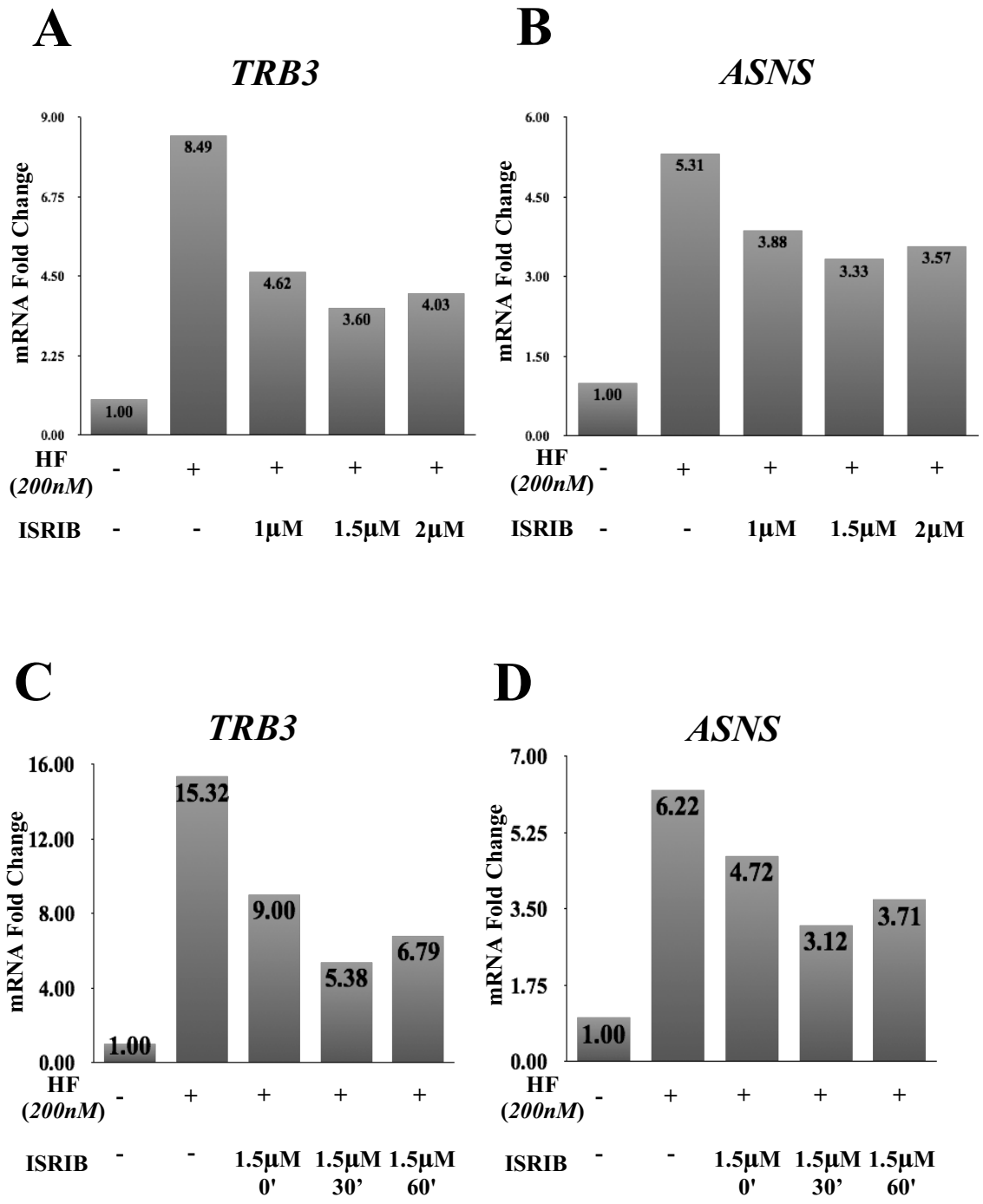

Figure 8: Assessing the ability of the small molecule, ISRIB, to block the induction of the AAR by HF in K4 synoviocytes at various ISRIB doses and pretreatment times.

(A-B) mRNA expression fold change of (A) TRB3 and (B) ASNS relative to the untreated control normalized to GAPDH. RNA was isolated from K4 synoviocytes that were serum starved for 24 hours followed by pre-treatment with three different doses of ISRIB for 30 minutes and then treatment with 250nM of HF for 4 hours. Results are representative of two independent experiments. (C-D) mRNA expression fold change of (C) TRB3 and (D) ASNS relative to the untreated control normalized to GAPDH. RNA was isolated from K4 synoviocytes that were serum starved for 24 hours followed by pre-treatment with 1.5μM of ISRIB for 0, 30, or 60 minutes followed by treatment with 250nM of HF for 4 hours. Results are representative of two independent experiments.

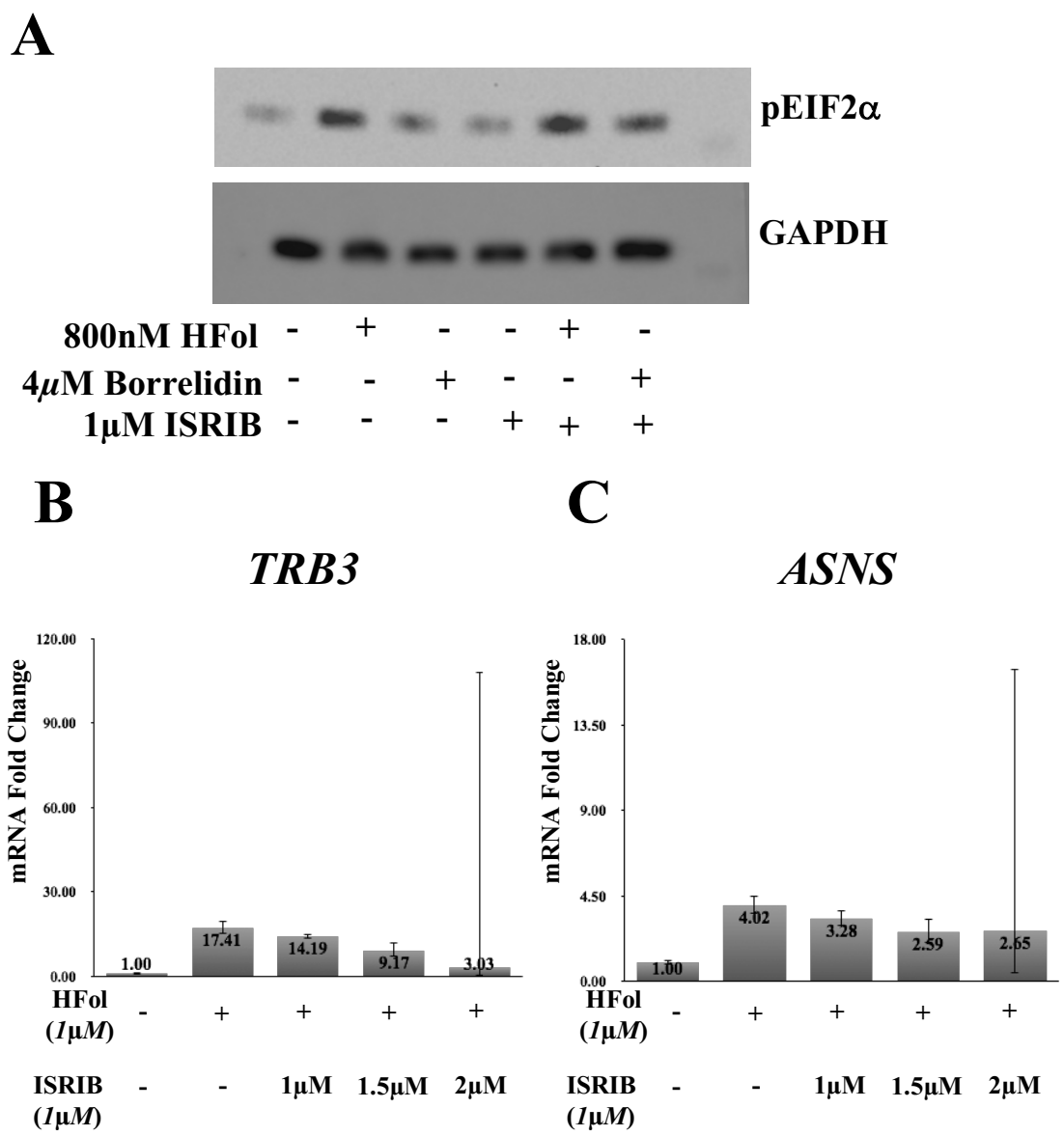

Figure 9: Assessing the ability of various doses of the small molecule, ISRIB, necessary to block the induction of AAR by HFol in LL29 fibroblasts.

(A) LL29 cells were treated with 1μM ISRIB for 30 minutes prior to treatment with either 800nM of HFol or 4μM of Borrelidin. Total protein lysates were immunoblotted for pEIF2a. GAPDH was used as the loading control. (B-C) mRNA expression fold change of (B)TRB3 and (C) ASNS relative to the untreated control normalized to GAPDH. Results are representative of three independent experiments.

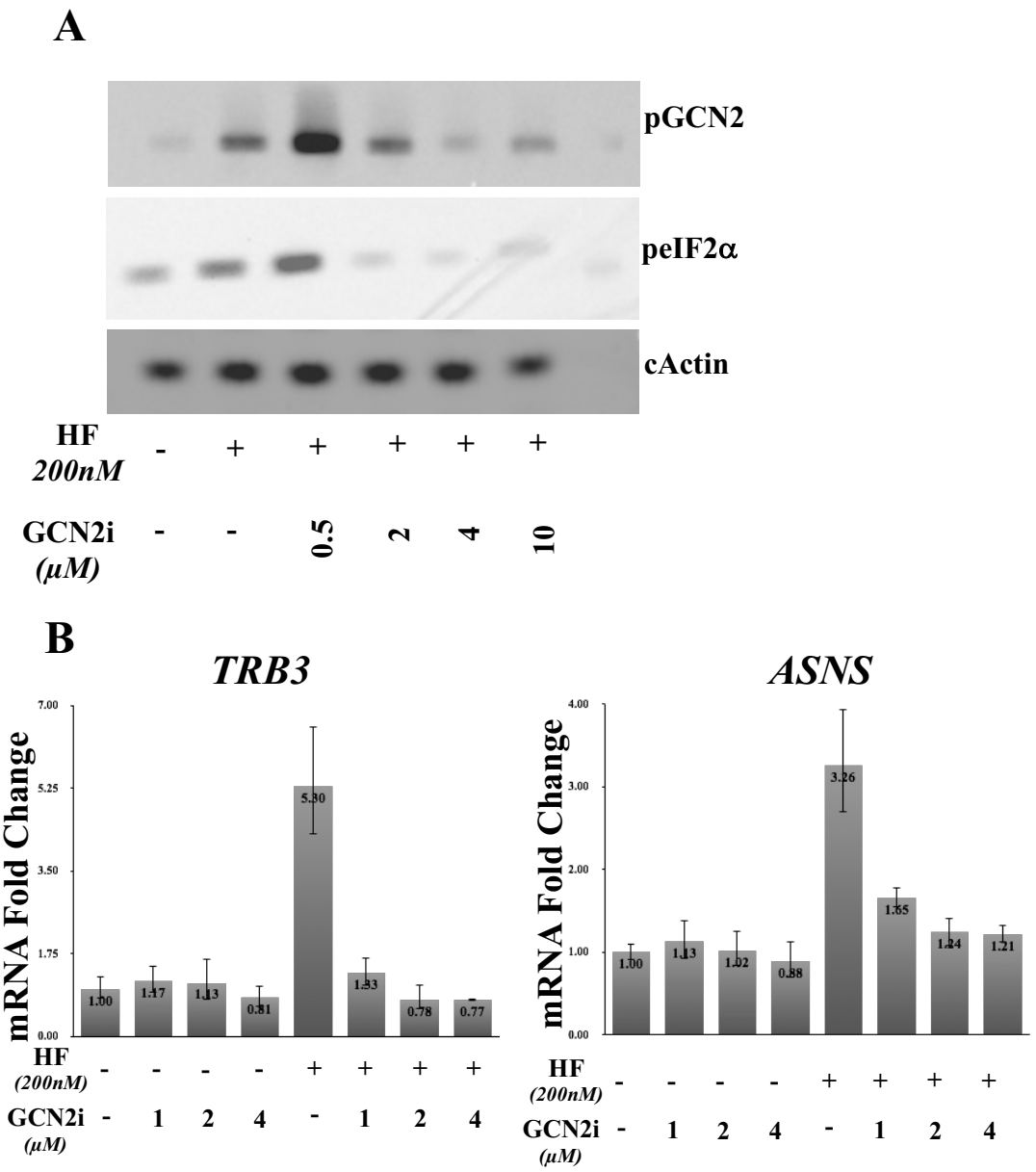

Figure 10: Establishing the dose range of GCN2i necessary to inhibit the HF-mediated induction of the AAR in K4 synoviocytes.

(A) K4 synoviocytes were treated for 30 minutes with 200nM HF and titrating doses (0.5μM to 10μM) of GCN2i. Total protein lysates were immunoblotted for phospho-GCN2 and phospho-eIF2α. Cytoplasmic actin (cActin) was the loading control. (B) K4 synoviocytes were treated with 200nM HF and titrating doses of GCN2i for 4 hours. Fold change gene expression of ATF4-regulated genes TRB3 and ASNS was measured.

GAPDH was used as the housekeeping gene. Results are representative of three independent experiments.

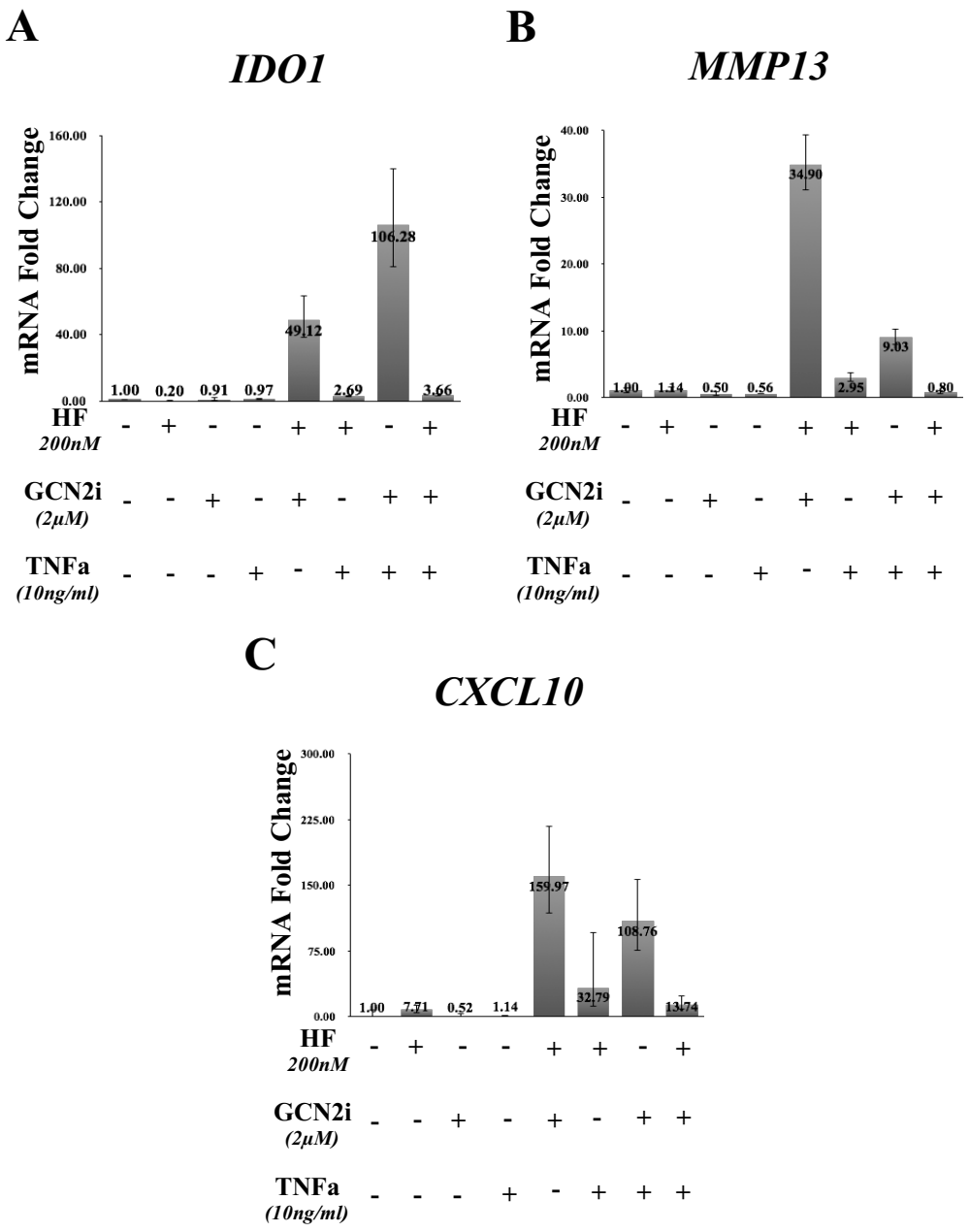

Figure 11: Assaying the effect of HF on TNFα-induced proinflammatory gene expression in the presence of GCN2i in K4 synoviocytes.

K4 synoviocytes were treated with 200nM HF and 2μM GCN2i for 16 hours followed by 10ng/mL TNFα treatment for 6 hours. Fold change expression of (A) MMP13, (B) IDO1 and (C) CXCL10 were measured relative to the untreated control. GAPDH was used as the housekeeping gene. Results are representative of three independent experiments.

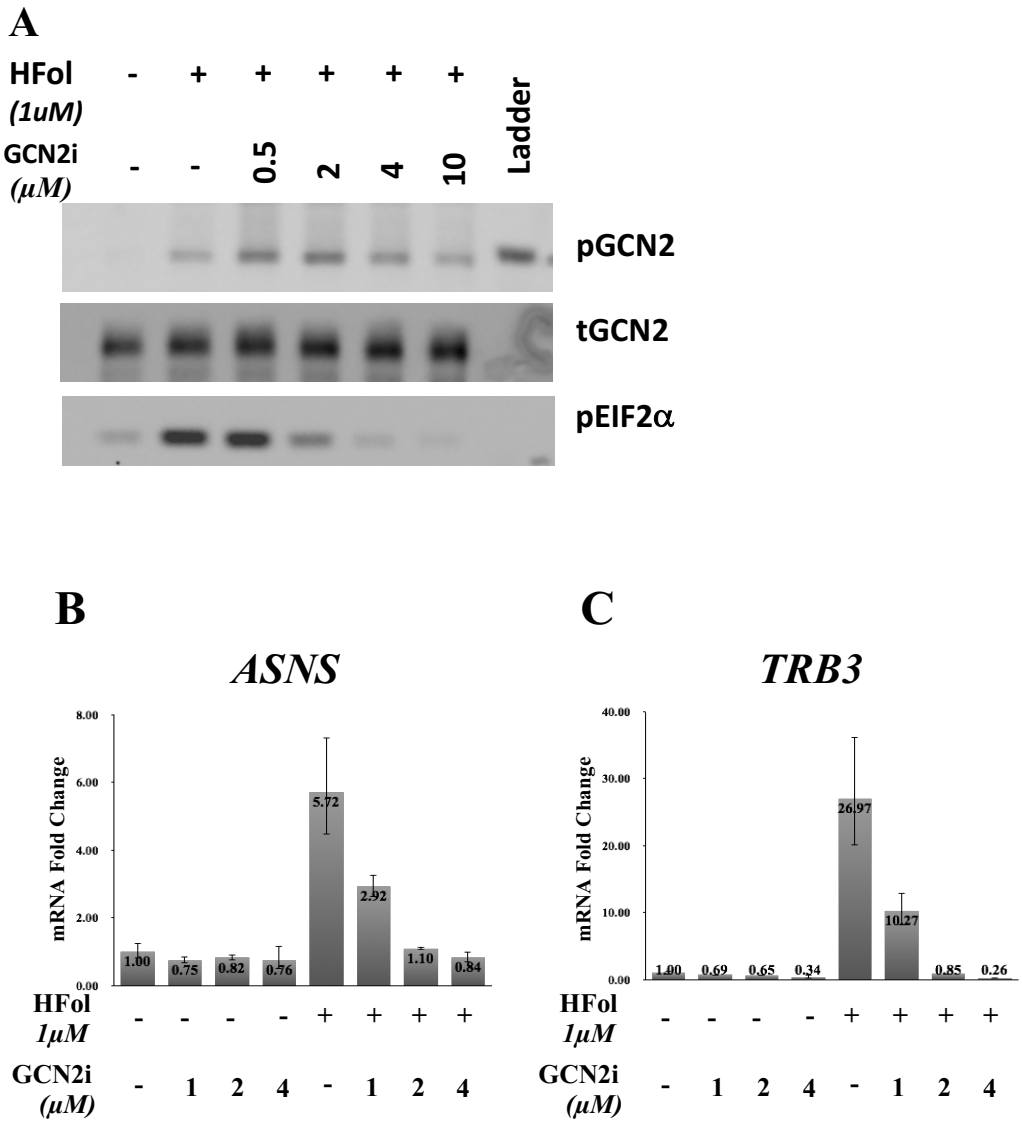

Figure 12: Establishing an effective dose range of GCN2i necessary to inhibit the AAR program that is induced by HFol in LL29 lung fibroblasts.

(A) LL29 fibroblasts were treated for 30 minutes with 1μM HFol and titrating doses of GCN2i. Total protein lysates were immunoblotted for phospho-GCN2, total-GCN2, and

phospho-eIF2α. Total-GCN2 was used as the loading control. (B-C) LL29 fibroblasts were treated with 1uM of HFol and titrating doses of GCN2i for 4 hours. mRNA fold change gene expression of ATF4-regulated genes (B)TRB3 and (C)ASNS was measured. GAPDH was used as the housekeeping gene. Results are representative of three independent experiments.

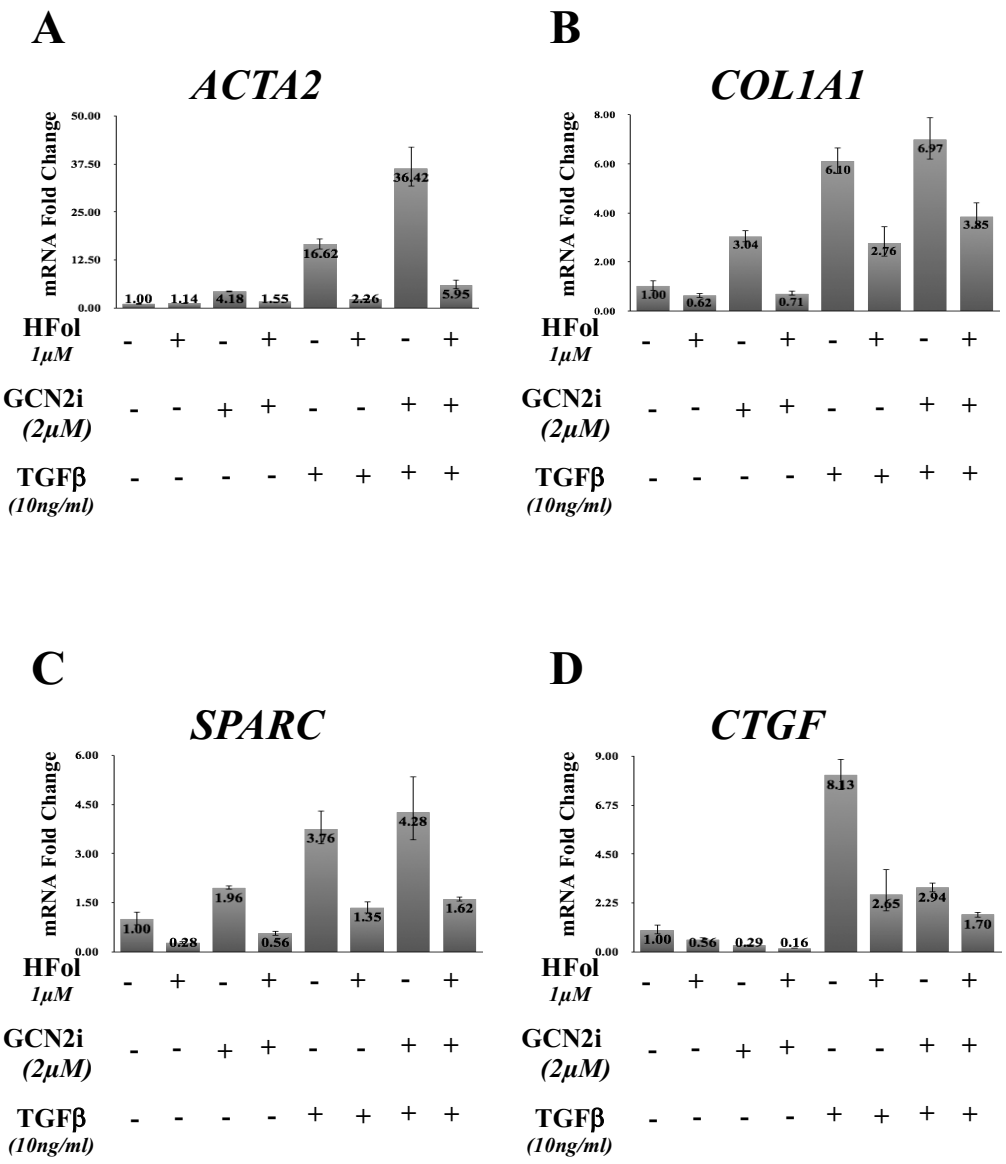

Figure 13: Assaying the effect of HFol on TGFβ-induced profibrotic gene expression in the presence of GCN2i.

mRNA Fold change expression of (A) ACTA2, (B)COL1A1, (C) SPARC, and (D) CTGF was measured relative to the untreated control. GAPDH was used as the housekeeping gene. Results are representative of three independent experiments.

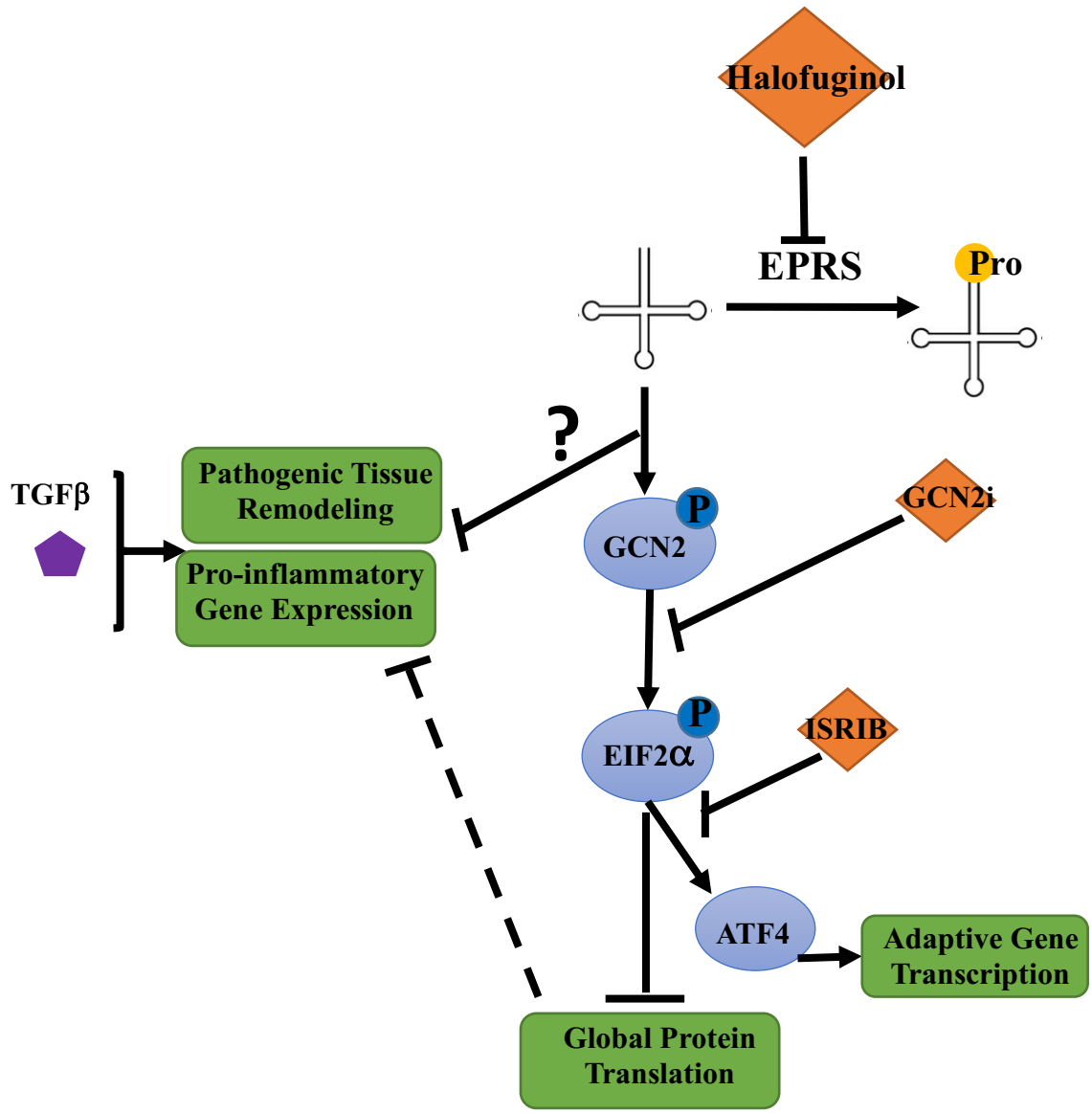

Figure 14: Working model of the mechanism of action of Halofuginol, a chemical derivative of HF, in the LL29 fibroblast.

Chapter IV.

Discussion

Interpretation of Results

The aims of this thesis were to characterize the transcriptional and translational responses to the small molecule inhibitor HFol and delineate the GCN2-independent effects of HFol in an in vitro cell culture system of TGFβ-stimulated pulmonary fibroblasts. The findings of this thesis deepen our understanding of the mechanisms behind HF-mediated effects on pulmonary fibrosis. Furthermore, this work finds that in addition to the prior work showing that HF can suppress the TNFα-mediated disease programs in synoviocytes (Kim et al, manuscript in preparation), HF can act directly on fibroblasts to suppress the profibrotic disease program activated by TGFβ. Cumulatively, the work presented in this thesis along with the work previously done by our group further establishes HF family members as suppressors of inflammatory responses orchestrated by various cytokines across a wide breadth of tissue targets pointing to a general mechanism of action of HF and its derivatives.

Similar to Kim et al (manuscript in preparation) with synovial cells, we showed that HF and the less toxic analog HFol activated the AAR in LL29 fibroblast. Interestingly, we showed that HFol can suppress TGFβ-induced transcriptional and translational programs in the LL29 cells, effects that can be reversed upon the addition of excess proline indicating the specificity of HFol to its target EPRS.

The global transcriptomic and proteomic profiling provided us with a comprehensive list of genes and proteins regulated by HFol in the presence of TGFβ. For

the most part the regulation by HFol at the transcriptional level was concordant with the regulation at the proteomic level. The transcriptomic and proteomic data also provided us with genes and proteins, whose expression was induced by TGFβ but remained unaffected by HFol. This data lends itself to the notion that HFol is modulating specific components of TGFβ-mediated profibrotic responses, ultimately conferring its therapeutic benefit.

A proposed model in the field is that HF exerts its anti-fibrotic effects by disrupting TGFβ-signaling through inhibition of Smad3 phosphorylation (Pines and Nagler 1998, McGaha 2002, Pines 2003). Nonetheless, the data presented here suggests that HFol does not affect the TGFβ-induced phosphorylation of Smad2 or Smad3 in LL29 cells. It is possible that HFol affects genes that are regulated by Smad activity and just not directly affects the activation of the Smad proteins in these cells. To investigate this, we should examine our transcriptomic for Smad-dependent genes to see how HFol affects their expression.

Finally, this study showed in the fibroblastic-system that HFol can suppress TGFβ-induced gene expression in the absence of GCN2 kinase activity. These findings indicate the novel, GCN2-independent, uncharged tRNA-sensing pathway identified in Kim et al (manuscript in preparation) is present and can be activated by HFol in the fibroblastic cell line LL29. While additional experiments need to be done to further validate and characterize how HF modulates different signaling pathways in a GCN2-independent manner, this thesis provides a preliminary examination of this phenomenon.

Limitations

To characterize the translational effects of HFol in TGFβ-stimulated LL29 cells we immunoblotted for canonical AAR markers, pGCN2 and peIF2α. We attempted to also immunoblot the samples for ATF4, the primary transcription factor of the AAR. However, we were unable to pick up consistent signal for ATF4 with our current antibody. My next step is to try a different commercially available antibody to detect the ATF4 expression as well as treat the LL29 cells for a longer period of time as ATF4 expression is known to be activated for up to 4 hours after the initial AAR activation.

The RNA-Seq and Proteomic assays were done on biological duplicate samples. While the assays provided us with a tangible and preliminary list of differentially expressed genes and proteins upon HFol treatment, we were unable to determine statistical significance from these arrays. It was confounding that only 4 of the top 50 genes were downregulated by HFol in TGFβ-stimulated cells relative to TGFβ-only treated LL29 cells. In the entire data set 300 of the total 18062 genes were suppressed at least two-fold in the presence of HFol and TGFβ relative to TGFβ-only treated samples (data not shown). It is possible that HFol affects TGFβ-stimulated gene expression earlier than the timepoints used in the RNA-Seq data. To that point, the follow-up qPCR analysis we performed, which used shorter timepoints and used biological triplicate samples, confirmed several of the transcriptional responses that came out of the RNA-Seq. Furthermore, we identified several genes that were affected by HFol at the protein level but not at the transcriptional level. One possibility for this discordance is that since there is a delay between the transcription of a gene and the translation of its product. Both

the transcriptomic and proteomic assays used the same timepoints, so it is possible we are not seeing correlating changes at the mRNA and protein level.

To first assess the GCN2-independent effects of HFol in this system, we applied the small molecule inhibitor, ISRIB. In the literature, ISRIB is regarded as a global ISR inhibitor that functions by reversing the translational effects conferred by the phosphorylation of EIF2α (Sidrauski 2015). However, we were unable to show that ISRIB suppressed HFol induction of pEIF2α in LL29 cells. Nonetheless, ISRIB would have only allowed us to investigate the effects of HFol independent of translational effects downstream of pEIF2a, not the complete GCN2-independent signaling cascade in response to HF and HFol.

When we used the GCN2 inhibitor, GCN2i, pGCN2 expression levels were irregular, this we used pEIF2α levels and the transcriptional upregulation of *ASNS* and *TRB3* as markers for AAR activation by HFol which were suppressed by GCN2i. The inconsistency in pGCN2 levels could be due to GCN2i solely inhibiting the kinase activity on eIF2α but not the autophosphorylation of GCN2. The small molecule was reported to inhibit GCN2 kinase activity with a 99.5% specificity but there were three other kinases that GCN2i showed >95% inhibition when used at 1μM (Nakamura 2018). These kinases were MAP2KS, STK10 and ZAK (Nakamura 2018). Since our assays applied more than 1μM, a possibility we cannot rule out is that GCN2i could be inhibiting other kinases aside from GCN2 in the LL29 cells. To validate that the effects of HFol indeed are GCN2-independent, future work should generate a GCN2-knockout in LL29 cells by CRISPR/Cas9 technology.

Future Directions

The results of this project further characterize the mechanism of action by which HFol can dampen a TGFβ-induced tissue remodeling program in a fibroblastic cell line. Nevertheless, additional work needs to be done to follow-up on the results presented here. The RNA-Seq and proteomic assays were done using timepoints that had long incubation periods with HFol. While HFol still appeared to be active in these samples, it is possible that HFol confers some of its therapeutic benefit at earlier timepoints. It would be useful to investigate the global programmatic response at earlier timepoints, to provide a more comprehensive view of the mechanism of HFol. Additionally, genes and proteins that have roles in the pathogenesis of fibrosis that have not been assayed in this work should be evaluated. This would continue to deepen our understanding of the different biological networks HFol can affect. The changes mediated by TGFβ and HFol at the protein level such as collagens, proteoglycans and actins are important to assess as these are the components that ultimately affect the pathogenesis of fibrosis.

We have also shown that HFol does not affect the TGFβ-induced phosphorylation of Smad2 or Smad3 in the LL29 cells. It has now been established that TGFβ signaling can act in a Smad-dependent or Smad-independent fashion (Dernyck 2003). It is possible that HFol affects gene regulation that is independent of Smad activity. Future work could assess the transcriptional responses of TGFβ-stimulated LL29 cells to HFol and SB431542 since SB431542 blocks Smad2 and Smad3 phosphorylation by inhibiting the ALK5 kinase receptor (Inman 2002).

We have shown here that HFol can dampen the transcriptional responses that are induced by TGFβ in the LL29 cells in a system devoid of GCN2 kinase activity. Next,

we need to evaluate how HFol affects the protein levels independent of GCN2 and if this correlates to what was observed at the transcriptional level. This is important because since fibrosis is the accumulation of the ECM components, we need to make sure that HFol is dampening the ECM protein accumulation.

In order to validate the results seen with the GCN2i, a GCN2-knockout LL29 cell line needs be generated. To do this we could use the CRIPSP/Cas9 system to generate a GCN2 knockout LL29 cell line. This cell line could then be used for RNA-Seq to assess the transcriptional response to HFol in a system that would lack an active AAR. Another option to further characterize the GCN2-independent pathway would be to use the GCN2-null mouse model (Munn 2005). The animal model would allow for us to investigate the GCN2-independent effects of HFol in a physiological relevant system. In addition, it would allow for us to observe the effects of HFol in a diverse tissue population rather than the artificial cell line system. To support the work of this thesis we could isolate pulmonary lung fibroblasts from GCN2-null mice and littermate controls and investigate the response to HFol in these cells.

While this study does not pinpoint the exact mechanism of action of HF and HFol, it does suggest HFol can confer therapeutic benefit independent of the AAR in a TGFβ-induced fibroblast. The novel GCN2-independent signaling pathway activated by HF is still being investigated. While we know HF and HFol inhibit EPRS to cause an accumulation of uncharged tRNAs and that downstream of this signal there is a dampening of pathogenic tissue remodeling programs, the intermediate steps remain elusive (Figure 14). One possibility is to identify regulatory sites that are shared amongst HFol-suppressed genes. To do this one could assay chromatin availability through

ATAC-Seq or assay protein-DNA binding through ChIP-Seq analysis. This would possibly shed some light, at the level of chromatin, on how HFol is able to function as a therapeutic for the plethora of diseases associated with pathological tissue remodeling.

References

Abramovitch, R., Dafni, H., Neeman, M., Nagler, A., & Pines, M. (1999). Inhibition of Neovascularization and Tumor Growth, Facilitation of Wound Repair, by Halofuginone, an Inhibitor of Collagen Type I Synthesis. *Neoplasia, 1*(4), 321-329. doi:https://doi.org/10.1038/sj.neo.7900043

Baird, T. D., & Wek, R. C. (2012). Eukaryotic initiation factor 2 phosphorylation and translational control in metabolism. *Adv Nutr, 3*(3), 307-321. doi:10.3945/an.112.002113

Bansal, R., Nakagawa, S., Yazdani, S., van Baarlen, J., Venkatesh, A., Koh, A. P., . . . Prakash, J. (2017). Integrin alpha 11 in the regulation of the myofibroblast phenotype: implications for fibrotic diseases. *Experimental &Amp; Molecular Medicine, 49*, e396. doi:10.1038/emm.2017.213

Barbosa, C., Peixeiro, I., & Romão, L. (2013). Gene Expression Regulation by Upstream Open Reading Frames and Human Disease. *PLOS Genetics, 9*(8), e1003529. doi:10.1371/journal.pgen.1003529

Bergmeier, V., Etich, J., Pitzler, L., Frie, C., Koch, M., Fischer, M., . . . Brachvogel, B. (2018). Identification of a myofibroblast-specific expression signature in skin wounds. *Matrix Biology, 65*, 59-74. doi:https://doi.org/10.1016/j.matbio.2017.07.005

Black, M., Milewski, D., Le, T., Ren, X., Xu, Y., Kalinichenko, V. V., & Kalin, T. V. (2018). FOXF1 Inhibits Pulmonary Fibrosis by Preventing CDH2-CDH11 Cadherin Switch in Myofibroblasts. *Cell Reports, 23*(2), 442-458. doi:10.1016/j.celrep.2018.03.067

Bruck, R., Genina, O., Aeed, H., Alexiev, R., Nagler, A., Avni, Y., & Pines, M. (2001). Halofuginone to prevent and treat thioacetamide-induced liver fibrosis in rats. *Hepatology, 33*(2), 379-386. doi:doi:10.1053/jhep.2001.21408

Castilho, B. A., Shanmugam, R., Silva, R. C., Ramesh, R., Himme, B. M., & Sattlegger, E. (2014). Keeping the eIF2 alpha kinase Gcn2 in check. *Biochim Biophys Acta, 1843*(9), 1948-1968. doi:10.1016/j.bbamcr.2014.04.006

Cipriani, P., Di Benedetto, P., Ruscitti, P., Liakouli, V., Berardicurti, O., Carubbi, F., . . . Giacomelli, R. (2016). Perivascular Cells in Diffuse Cutaneous Systemic Sclerosis Overexpress Activated ADAM12 and Are Involved in Myofibroblast Transdifferentiation and Development of Fibrosis. *The Journal of Rheumatology, 43*(7), 1340. doi:10.3899/jrheum.150996

Connor, J. H., Weiser, D. C., Li, S., Hallenbeck, J. M., & Shenolikar, S. (2001). Growth Arrest and DNA Damage-Inducible Protein GADD34 Assembles a Novel

Signaling Complex Containing Protein Phosphatase 1 and Inhibitor 1. *Molecular and Cellular Biology, 21*(20), 6841. doi:10.1128/MCB.21.20.6841-6850.2001

Correll, K. A., Edeen, K. E., Redente, E. F., Zemans, R. L., Edelman, B. L., Danhorn, T., . . . Mason, R. J. (2018). TGF beta inhibits HGF, FGF7, and FGF10 expression in normal and IPF lung fibroblasts. *Physiological reports, 6*(16), e13794-e13794. doi:10.14814/phy2.13794

Cully, M. (2016). CXCR7 activation overrides lung fibrosis. *Nature Reviews Drug Discovery, 15*, 160. doi:10.1038/nrd.2016.25

De Minicis, S., Rychlicki, C., Agostinelli, L., Saccomanno, S., Trozzi, L., Candelaresi, C., . . . Svegliati-Baroni, G. (2013). Semaphorin 7A Contributes to TGF-β-Mediated Liver Fibrogenesis. *The American Journal of Pathology, 183*(3), 820-830. doi:10.1016/j.ajpath.2013.05.030

Demonbreun, A. R., Allen, M. V., Warner, J. L., Barefield, D. Y., Krishnan, S., Swanson, K. E., . . . McNally, E. M. (2016). Enhanced Muscular Dystrophy from Loss of Dysferlin Is Accompanied by Impaired Annexin A6 Translocation after Sarcolemmal Disruption. *The American Journal of Pathology, 186*(6), 1610-1622. doi:10.1016/j.ajpath.2016.02.005

Derynck, R., & Zhang, Y. E. (2003). Smad-dependent and Smad-independent pathways in TGF-β family signaling. *Nature, 425*, 577. doi:10.1038/nature02006

Dong, J., Qiu, H., Garcia-Barrio, M., Anderson, J., & Hinnebusch, A. G. (2000). Uncharged tRNA Activates GCN2 by Displacing the Protein Kinase Moiety from a Bipartite tRNA-Binding Domain. *Molecular Cell, 6*(2), 269-279. doi:https://doi.org/10.1016/S1097-2765(00)00028-9

Efeyan, A., Comb, W. C., & Sabatini, D. M. (2015). Nutrient-sensing mechanisms and pathways. *Nature, 517*, 302. doi:10.1038/nature14190

Elkin, M., Reich, R., Nagler, A., Aingorn, E., Pines, M., de-Groot, N., . . . Vlodavsky, I. (1999). Inhibition of Matrix Metalloproteinase-2 Expression and Bladder Carcinoma Metastasis by Halofuginone. *Clinical Cancer Research, 5*(8), 1982.

Galán-Cobo, A., Arellano-Orden, E., Sánchez Silva, R., López-Campos, J. L., Gutiérrez Rivera, C., Gómez Izquierdo, L., . . . Echevarría, M. (2018). The Expression of AQP1 IS Modified in Lung of Patients With Idiopathic Pulmonary Fibrosis: Addressing a Possible New Target. *Frontiers in Molecular Biosciences, 5*(43). doi:10.3389/fmolb.2018.00043

Gallinetti, J., Harputlugil, E., & Mitchell, J. R. (2013). Amino acid sensing in dietary-restriction-mediated longevity: roles of signal-transducing kinases GCN2 and TOR. *Biochem J, 449*(1), 1-10. doi:10.1042/BJ20121098

Habibi, D., Ogloff, N., Jalili, R. B., Yost, A., Weng, A. P., Ghahary, A., & Ong, C. J. (2012). Borrelidin, a small molecule nitrile-containing macrolide inhibitor of threonyl-tRNA synthetase, is a potent inducer of apoptosis in acute lymphoblastic leukemia. *Investigational New Drugs, 30*(4), 1361-1370. doi:10.1007/s10637-011-9700-y

Harding, H. P., Zhang, Y., Zeng, H., Novoa, I., Lu, P. D., Calfon, M., . . . Ron, D. (2003). An Integrated Stress Response Regulates Amino Acid Metabolism and Resistance to Oxidative Stress. *Molecular Cell, 11*(3), 619-633. doi:10.1016/s1097-2765(03)00105-9

Hinnebusch, A. G. (2005). Translational regulation of gcn4 and the general amino acid control of yeast. *Annual Review of Microbiology, 59*(1), 407-450. doi:10.1146/annurev.micro.59.031805.133833

Hotta, Y., Uchiyama, K., Takagi, T., Kashiwagi, S., Nakano, T., Mukai, R., . . . Itoh, Y. (2018). Transforming growth factor β1-induced collagen production in myofibroblasts is mediated by reactive oxygen species derived from NADPH oxidase 4. *Biochemical and Biophysical Research Communications, 506*(3), 557-562. doi:https://doi.org/10.1016/j.bbrc.2018.10.116

Huebner, K. D., Jassal, D. S., Halevy, O., Pines, M., & Anderson, J. E. (2008). Functional resolution of fibrosis in mdx mouse dystrophic heart and skeletal muscle by halofuginone. *American Journal of Physiology-Heart and Circulatory Physiology, 294*(4), H1550-H1561. doi:10.1152/ajpheart.01253.2007

Ibba, M., & Söll, D. (2000). Aminoacyl-tRNA Synthesis. *Annual Review of Biochemistry, 69*(1), 617-650. doi:10.1146/annurev.biochem.69.1.617

Inman, G. J., Nicolás, F. J., Callahan, J. F., Harling, J. D., Gaster, L. M., Reith, A. D., . . . Hill, C. S. (2002). SB-431542 Is a Potent and Specific Inhibitor of Transforming Growth Factor-β Superfamily Type I Activin Receptor-Like Kinase (ALK) Receptors ALK4, ALK5, and ALK7. *Molecular Pharmacology, 62*(1), 65. doi:10.1124/mol.62.1.65

Jousse, C., Deval, C., Maurin, A.-C., Parry, L., Chérasse, Y., Chaveroux, C., . . . Fafournoux, P. (2007). TRB3 Inhibits the Transcriptional Activation of Stress-regulated Genes by a Negative Feedback on the ATF4 Pathway. *Journal of Biological Chemistry, 282*(21), 15851-15861. doi:10.1074/jbc.M611723200

Keller, T. L., Zocco, D., Sundrud, M. S., Hendrick, M., Edenius, M., Yum, J., . . . Whitman, M. (2012). Halofuginone and other febrifugine derivatives inhibit prolyl-tRNA synthetase. *Nat Chem Biol, 8*(3), 311-317. doi:10.1038/nchembio.790

Kilberg, M. S., Pan, Y. X., Chen, H., & Leung-Pineda, V. (2005). Nutritional control of gene expression: How Mammalian Cells Respond to Amino Acid Limitation.

Annual Review of Nutrition, 25(1), 59-85. doi:10.1146/annurev.nutr.24.012003.132145

Kilberg, M. S., Shan, J., & Su, N. (2009). ATF4-dependent transcription mediates signaling of amino acid limitation. *Trends in Endocrinology & Metabolism, 20*(9), 436-443. doi:10.1016/j.tem.2009.05.008

Kilberg, M. S., Balasubramanian, M., Fu, L., & Shan, J. (2012). The Transcription Factor Network Associated With the Amino Acid Response in Mammalian Cells. *Advances in Nutrition, 3*(3), 295-306. doi:10.3945/an.112.001891

Lageix, S., Zhang, J., Rothenburg, S., & Hinnebusch, A. G. (2015). Interaction between the tRNA-Binding and C-Terminal Domains of Yeast Gcn2 Regulates Kinase Activity In Vivo. *PLOS Genetics, 11*(2), e1004991. doi:10.1371/journal.pgen.1004991

Lei, G.-S., Kline, H. L., Lee, C.-H., Wilkes, D. S., & Zhang, C. (2016). Regulation of Collagen V Expression and Epithelial-Mesenchymal Transition by miR-185 and miR-186 during Idiopathic Pulmonary Fibrosis. *The American Journal of Pathology, 186*(9), 2310-2316. doi:10.1016/j.ajpath.2016.04.015

Levi-Schaffer, F., Nagler, A., Slavin, S., Knopov, V., & Pines, M. (1996). Inhibition of Collagen Synthesis and Changes in Skin Morphology in Murine Graft-Versus-Host Disease and Tight Skin Mice: Effect of Halofuginone. *Journal of Investigative Dermatology, 106*(1), 84-88. doi:https://doi.org/10.1111/1523-1747.ep12328014

Li, X., Zhao, D., Guo, Z., Li, T., Qili, M., Xu, B., . . . Shan, H. (2016). Overexpression of SerpinE2/protease nexin-1 Contribute to Pathological Cardiac Fibrosis via increasing Collagen Deposition. *Scientific Reports, 6*, 37635. doi:10.1038/srep37635

Luo, Y., Xie, X., Luo, D., Wang, Y., & Gao, Y. (2017). The role of halofuginone in fibrosis: more to be explored? *J Leukoc Biol, 102*(6), 1333-1345. doi:10.1189/jlb.3RU0417-148RR

McGaha, T. L., Bona, C., Phelps, R. G., & Spiera, H. (2002). Halofuginone, an Inhibitor of Type-I Collagen Synthesis and Skin Sclerosis, Blocks Transforming-Growth-Factor-β-Mediated Smad3 Activation in Fibroblasts. *Journal of Investigative Dermatology, 118*(3), 461-470. doi:10.1046/j.0022-202x.2001.01690.x

McInnes, I. B., & Schett, G. (2011). The Pathogenesis of Rheumatoid Arthritis. *New England Journal of Medicine, 365*(23), 2205-2219. doi:10.1056/NEJMra1004965

Munn, D. H., Sharma, M. D., Baban, B., Harding, H. P., Zhang, Y., Ron, D., & Mellor, A. L. (2005). GCN2 Kinase in T Cells Mediates Proliferative Arrest and Anergy Induction in Response to Indoleamine 2,3-Dioxygenase. *Immunity, 22*(5), 633-642. doi:https://doi.org/10.1016/j.immuni.2005.03.013

Nakano, N., Maeyama, K., Sakata, N., Itoh, F., Akatsu, R., Nakata, M., . . . Itoh, S. (2014). C18 ORF1, a Novel Negative Regulator of Transforming Growth Factor-β Signaling. *Journal of Biological Chemistry, 289*(18), 12680-12692. doi:10.1074/jbc.M114.558981

Nakayama, Y., Tsuruya, Y., Noda, K., Yamazaki-Takai, M., Iwai, Y., Ganss, B., & Ogata, Y. (2018). Negative feedback by SNAI2 regulates TGFβ1-induced amelotin gene transcription in epithelial–mesenchymal transition. *Journal of Cellular Physiology, 0*(0). doi:10.1002/jcp.27804

Nanthakumar, C. B., Hatley, R. J. D., Lemma, S., Gauldie, J., Marshall, R. P., & Macdonald, S. J. F. (2015). Dissecting fibrosis: therapeutic insights from the small-molecule toolbox. *Nature Reviews Drug Discovery, 14*(10), 693-720. doi:10.1038/nrd4592

Oishi, H., Martinu, T., Sato, M., Matsuda, Y., Hirayama, S., Juvet, S. C., . . . Keshavjee, S. (2016). Halofuginone treatment reduces interleukin-17A and ameliorates features of chronic lung allograft dysfunction in a mouse orthotopic lung transplant model. *J Heart Lung Transplant, 35*(4), 518-527. doi:10.1016/j.healun.2015.12.003

Pakos-Zebrucka, K., Koryga, I., Mnich, K., Ljujic, M., Samali, A., & Gorman, A. M. (2016). The integrated stress response. *EMBO reports, 17*(10), 1374. doi:10.15252/embr.201642195

Pilewski, J. M., Liu, L., Henry, A. C., Knauer, A. V., & Feghali-Bostwick, C. A. (2005). Insulin-Like Growth Factor Binding Proteins 3 and 5 Are Overexpressed in Idiopathic Pulmonary Fibrosis and Contribute to Extracellular Matrix Deposition. *The American Journal of Pathology, 166*(2), 399-407. doi:10.1016/S0002-9440(10)62263-8

Pines, M., & Nagler, A. (1998). Halofuginone: A Novel Antifibrotic Therapy. *General Pharmacology: The Vascular System, 30*(4), 445-450. doi:https://doi.org/10.1016/S0306-3623(97)00307-8

Pines, M., Snyder, D., Yarkoni, S., & Nagler, A. (2003). Halofuginone to treat fibrosis in chronic graft-versus-host disease and scleroderma. *Biology of Blood and Marrow Transplantation, 9*(7), 417-425. doi:10.1016/S1083-8791(03)00151-4

Pines, M., & Spector, I. (2015). Halofuginone - the multifaceted molecule. *Molecules, 20*(1), 573-594. doi:10.3390/molecules20010573

Qin, P., Arabacilar, P., Bernard, R. E., Bao, W., Olzinski, A. R., Guo, Y., . . . Willette, R. N. (2017). Activation of the Amino Acid Response Pathway Blunts the Effects of Cardiac Stress. *Journal of the American Heart Association, 6*(5). doi:10.1161/jaha.116.004453

Rockey, D. C., Bell, P. D., & Hill, J. A. (2015). Fibrosis--a common pathway to organ injury and failure. *N Engl J Med, 372*(12), 1138-1149. doi:10.1056/NEJMra1300575

Roffe, S., Hagai, Y., Pines, M., & Halevy, O. (2010). Halofuginone inhibits Smad3 phosphorylation via the PI3K/Akt and MAPK/ERK pathways in muscle cells: Effect on myotube fusion. *Experimental Cell Research, 316*(6), 1061-1069. doi:https://doi.org/10.1016/j.yexcr.2010.01.003

Ruiz, X. D., Mlakar, L. R., Yamaguchi, Y., Su, Y., Larregina, A. T., Pilewski, J. M., & Feghali-Bostwick, C. A. (2012). Syndecan-2 Is a Novel Target of Insulin-Like Growth Factor Binding Protein-3 and Is Over-Expressed in Fibrosis. *PLOS ONE, 7*(8), e43049. doi:10.1371/journal.pone.0043049

Ryley, J. F., & Betts, M. J. (1973). Chemotherapy of chicken coccidiosis. In Advances in Pharmacology (11), 221-293. Elsevier.

Schafer, S., Viswanathan, S., Widjaja, A. A., Lim, W.-W., Moreno-Moral, A., DeLaughter, D. M., . . . Cook, S. A. (2017). IL-11 is a crucial determinant of cardiovascular fibrosis. *Nature, 552*, 110. doi:10.1038/nature24676

Schulz, J.-N., Nüchel, J., Niehoff, A., Bloch, W., Schönborn, K., Hayashi, S., . . . Eckes, B. (2016). COMP-assisted collagen secretion – a novel intracellular function required for fibrosis. *Journal of Cell Science, 129*(4), 706. doi:10.1242/jcs.180216

Selman, M., Ruiz, V., Cabrera, S., Segura, L., Ramírez, R., Barrios, R., & Pardo, A. (2000). TIMP-1, -2, -3, and -4 in idiopathic pulmonary fibrosis. A prevailing nondegradative lung microenvironment? *American Journal of Physiology-Lung Cellular and Molecular Physiology, 279*(3), L562-L574. doi:10.1152/ajplung.2000.279.3.L562

Shibata, A., Kuno, M., Adachi, R., Sato, Y., Hattori, H., Matsuda, A., . . . Okaniwa, M. (2017). Discovery and pharmacological characterization of a new class of prolyl-tRNA synthetase inhibitor for anti-fibrosis therapy. *PloS one, 12*(10), e0186587-e0186587. doi:10.1371/journal.pone.0186587

Spanjer, A. I. R., Baarsma, H. A., Oostenbrink, L. M., Jansen, S. R., Kuipers, C. C., Lindner, M., . . . Königshoff, M. (2016). TGF-β-induced profibrotic signaling is regulated in part by the WNT receptor Frizzled-8. *The FASEB Journal, 30*(5), 1823-1835. doi:10.1096/fj.201500129

Sundrud, M. S., Koralov, S. B., Feuerer, M., Calado, D. P., Kozhaya, A. E., Rhule-Smith, A., . . . Rao, A. (2009). Halofuginone inhibits TH17 cell differentiation by activating the amino acid starvation response. *Science, 324*(5932), 1334-1338. doi:10.1126/science.1172638

Szklarczyk, D., Morris, J. H., Cook, H., Kuhn, M., Wyder, S., Simonovic, M., . . . von Mering, C. (2017). The STRING database in 2017: quality-controlled protein-

protein association networks, made broadly accessible. *Nucleic acids research, 45*(D1), D362-D368. doi:10.1093/nar/gkw937

Turgeman, T., Hagai, Y., Huebner, K., Jassal, D. S., Anderson, J. E., Genin, O., . . . Pines, M. (2008). Prevention of muscle fibrosis and improvement in muscle performance in the mdx mouse by halofuginone. *Neuromuscular Disorders, 18*(11), 857-868. doi:10.1016/j.nmd.2008.06.386

van Caam, A., Madej, W., Garcia de Vinuesa, A., Goumans, M.-J., Ten Dijke, P., Blaney Davidson, E., & van der Kraan, P. (2017). TGFβ1-induced SMAD2/3 and SMAD1/5 phosphorylation are both ALK5-kinase-dependent in primary chondrocytes and mediated by TAK1 kinase activity. *Arthritis research & therapy, 19*(1), 112-112. doi:10.1186/s13075-017-1302-4

Verrecchia, F., & Mauviel, A. (2002). Transforming Growth Factor-β Signaling Through the Smad Pathway: Role in Extracellular Matrix Gene Expression and Regulation. *Journal of Investigative Dermatology, 118*(2), 211-215. doi:https://doi.org/10.1046/j.1523-1747.2002.01641.x

Wang, M., Gong, Q., Zhang, J., Chen, L., Zhang, Z., Lu, L., . . . Zhang, X. (2017). Characterization of gene expression profiles in HBV-related liver fibrosis patients and identification of ITGBL1 as a key regulator of fibrogenesis. *Scientific Reports, 7*, 43446. doi:10.1038/srep43446

Wynn, T. A. (2008). Cellular and molecular mechanisms of fibrosis. *J Pathol, 214*(2), 199-210. doi:10.1002/path.2277

Zeng, X., Huang, C., Senavirathna, L., Wang, P., & Liu, L. (2017). miR-27b inhibits fibroblast activation via targeting TGFβ signaling pathway. *BMC Cell Biology, 18*(1), 9. doi:10.1186/s12860-016-0123-7

Zion, O., Genin, O., Kawada, N., Yoshizato, K., Roffe, S., Nagler, A., . . . Pines, M. (2009). Inhibition of Transforming Growth Factor β Signaling by Halofuginone as a Modality for Pancreas Fibrosis Prevention. *Pancreas, 38*(4), 427-435. doi:10.1097/MPA.0b013e3181967670